Deep Learning in Quantitative SPECT and PET Image Reconstruction and Processing

Chi Liu, PhD
Associate Professor
Radiology and Biomedical Imaging
Biomedical Engineering
Yale University

Outline

- SPECT
  - Attenuation Map Generation
  - Attenuation Correction
- PET
  - Denoising
  - Motion Correction
  - Multi-tracer Image Generation

Background and Motivation

- Accurate attenuation correction (AC) is essential for SPECT

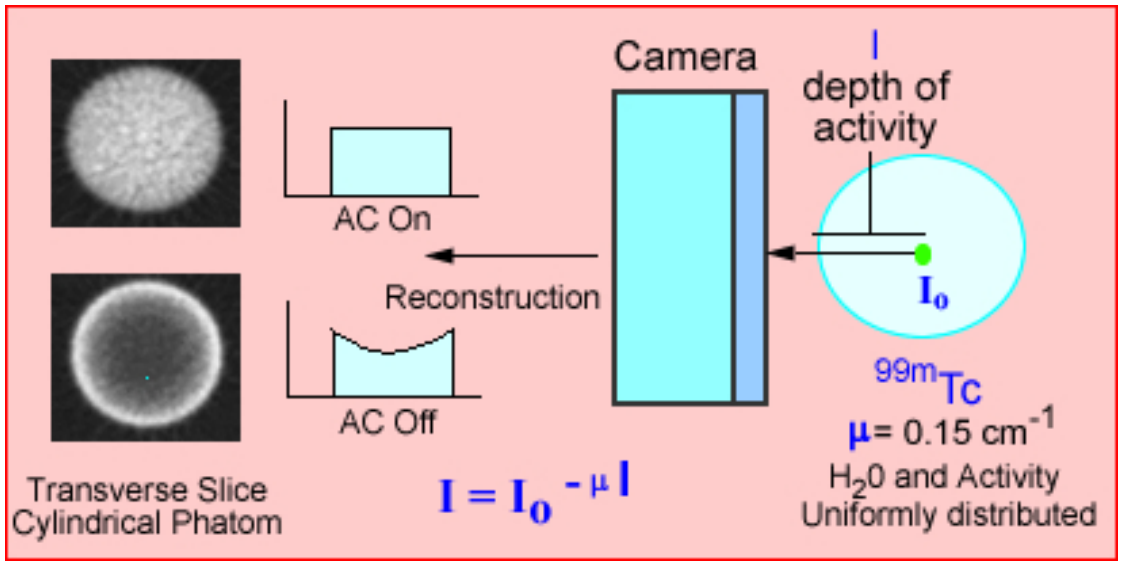

Daisuke Utsunomiya, et al. Object-specific Attenuation Correction at SPECT/CT in Thorax: Optimization of Respiratory Protocol for Image Registration

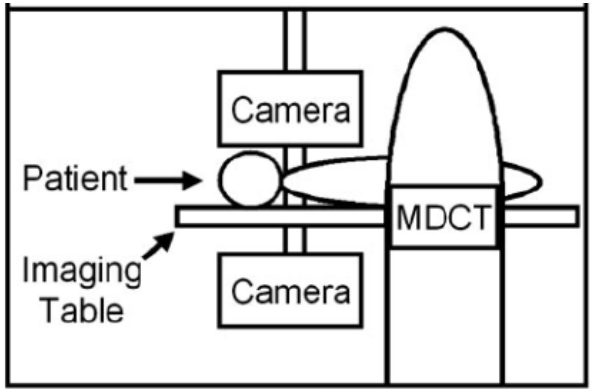

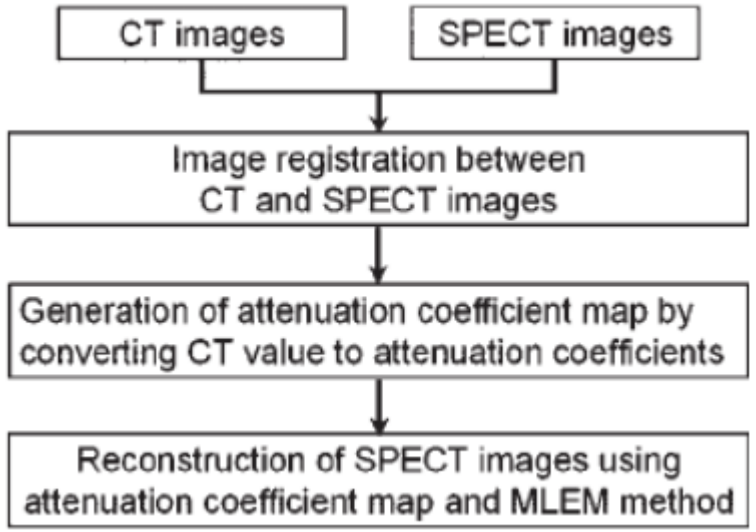

http://www.people.vcu.edu/~mhcrosthwait/clrs318web/AC%20and%20transmission%20applicatiin.html

GAN Training and Human Studies

- Generator : U-net 3D
- Discriminator: CNN 3D
- 65 patient studies from YNHH
- Cardiac SPECT with ^{99m}Tc-tetrofosmin and attenuation CT scans
- GE Discovery NM/CT 850
  - Primary: 126 keV-155 keV
  - Scatter: 114 keV-126 keV

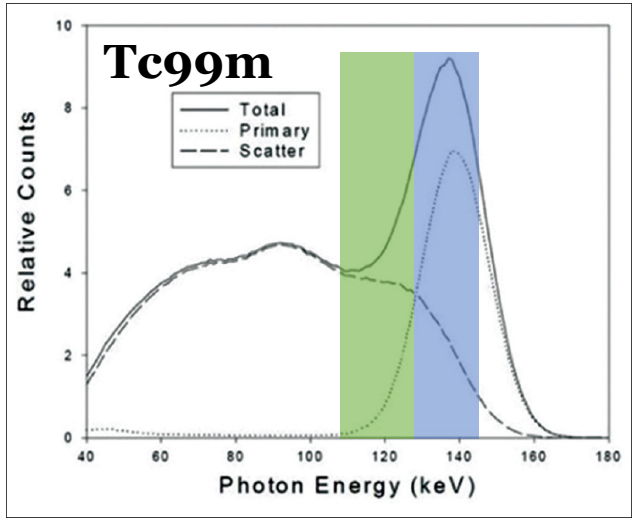

scatter window (114keV-126keV)

primary window (126keV-155keV)

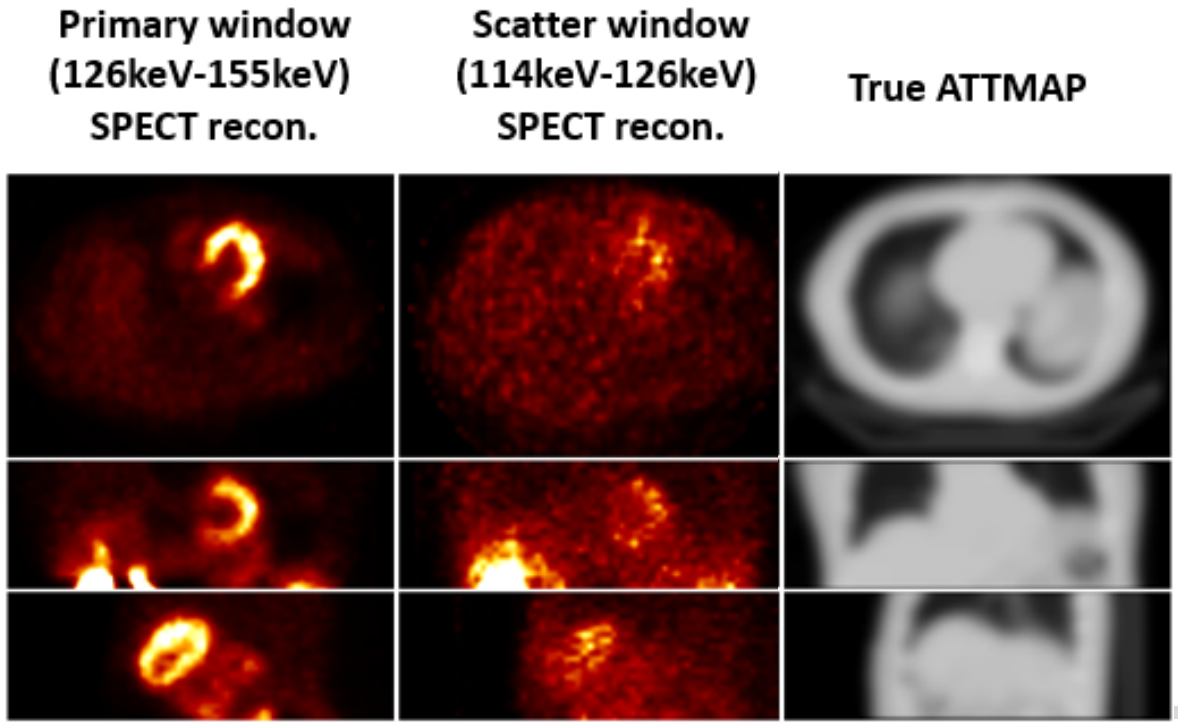

L. Shi, et al. SNMMI 2019

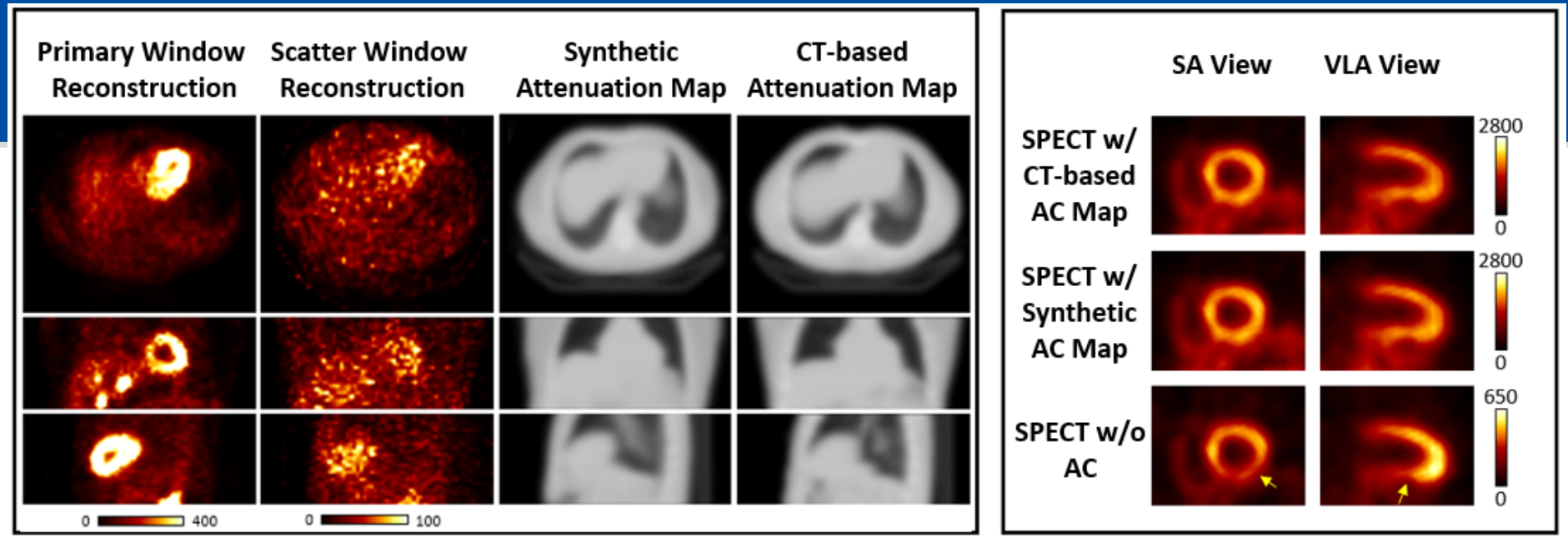

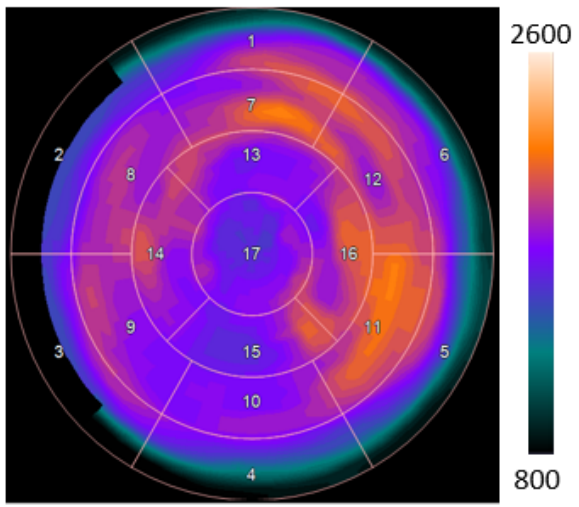

SPECT w/ CT-based AC Map

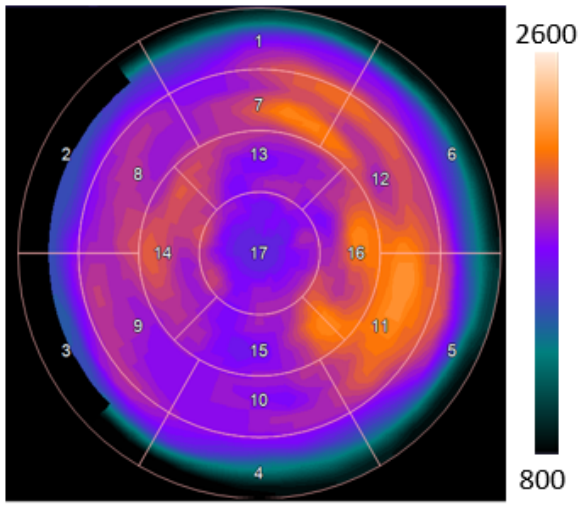

SPECT w/ Synthetic AC Map

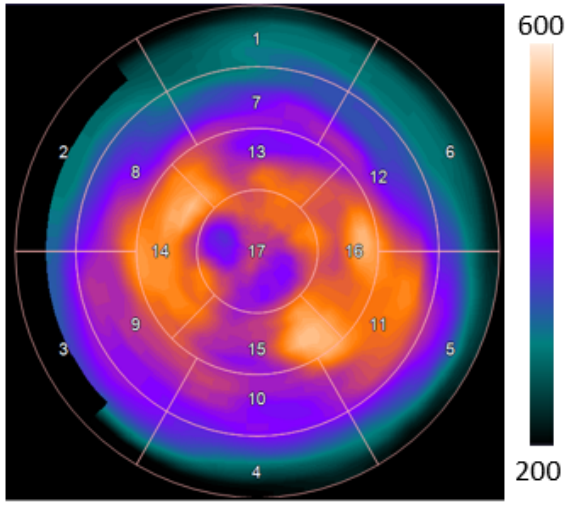

SPECT w/o AC

Impact of Multi-channel Inputs and GAN

- Inaccurate body boundary recovery and artifacts (red arrows) were observed in GAN-P and UNET-P's results
- Incorrect blood vessel shape was observed (yellow arrows) in the results from GAN-S and UNET-S
- When using only the primary window as input, GAN obtained much better result than U-net

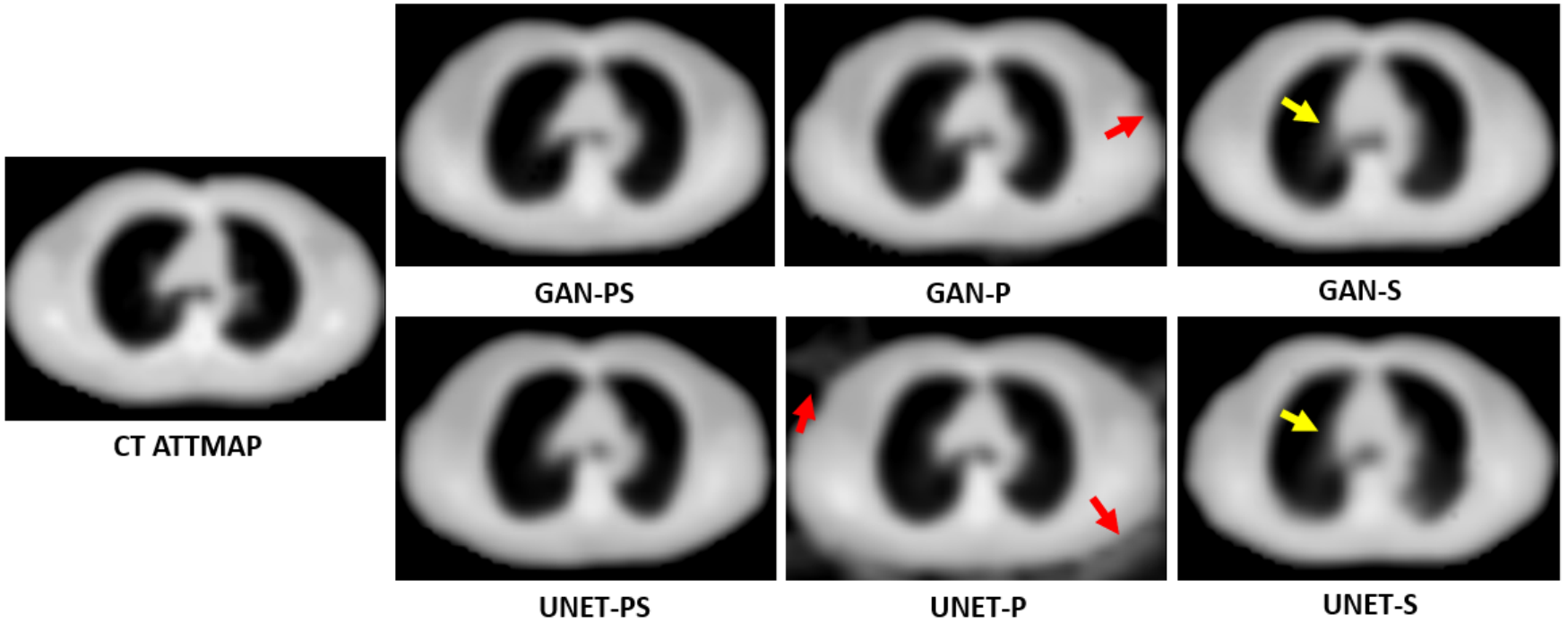

Visual comparison of GAN and U-Net using different inputs: both primary and scatter windows (PS), primary window alone (P) and scatter window alone (S).

Evaluation

Metric	GAN-PS	GAN-P	GAN-S	UNET-PS	UNET-P	UNET-S
%NMAE-μ	**3.60±0.85**	5.12±1.03	3.62±0.86	**3.60±0.85**	24.3±1.76	3.65±0.82
MSE-μ	189±89	270±123	192±94	**185±92**	2594±207	190±89
%NMAE-λ	**0.26±0.15**	0.30±0.17	0.27±0.16	**0.26±0.15**	0.92±0.48	0.27±0.16
$\%Bias_{myo}$	**3.48±2.05**	5.75±3.39	4.36±2.54	3.81±2.13	37.9±9.84	3.67±2.45
$\%Bias_{blp}$	**2.43±1.42**	4.34±3.04	2.69±2.06	2.49±1.52	31.5±9.08	2.46±1.86

- UNET-P produced the worst results
- The GAN counterpart (GAN-P) produced more stable results
- The GAN-PS, GAN-S, UNET-PS and UNET-S methods obtained similar NMAE and MSE on the generated attenuation maps (μ) and attenuation corrected SPECT images (λ).
- GAN-PS achieved the lowest ROI bias among all the methods
- For both GAN and U-net, the STD of bias are much lower when both primary and scatter windows were used as input, compared with the results based only on scatter input.

PET dose reduction

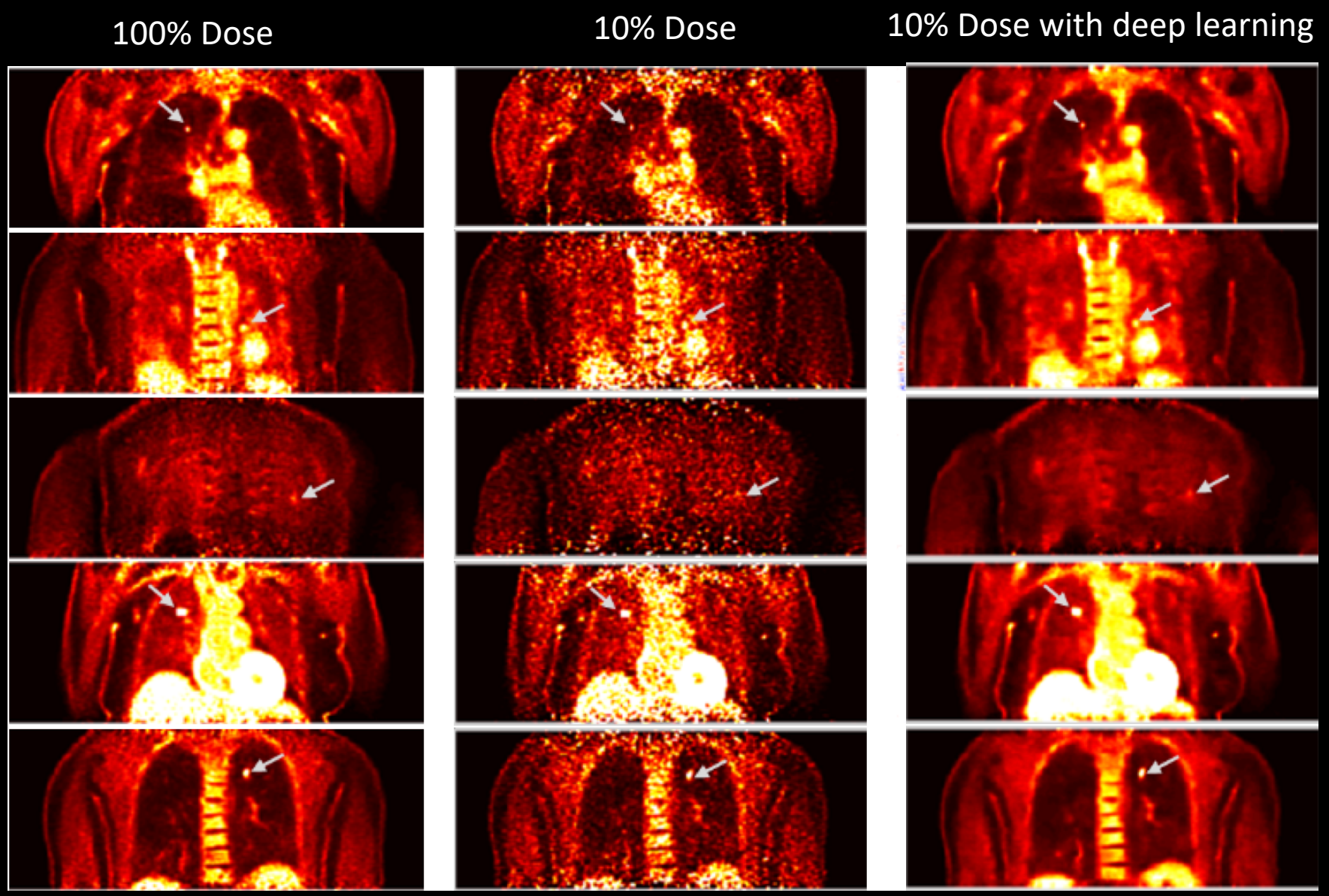

W. Lu, et al. PMB 2019

Comparison with existing denoising methods

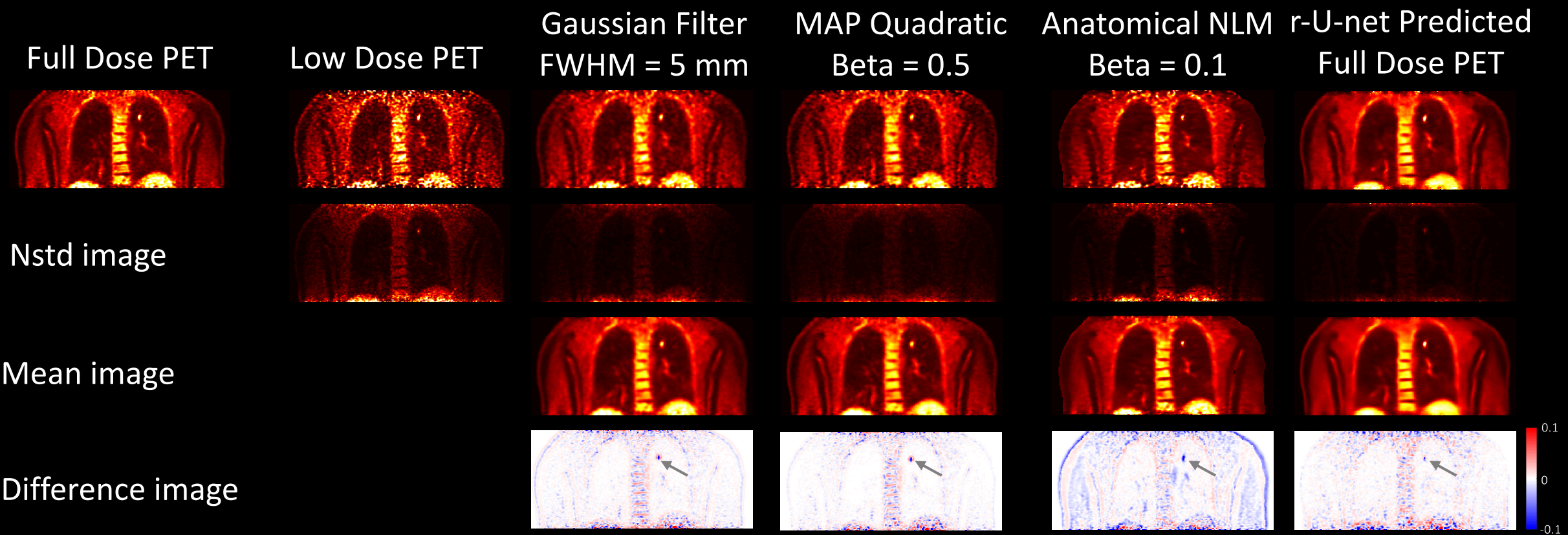

W. Lu, et al. PMB 2019

Comparison with existing denoising methods

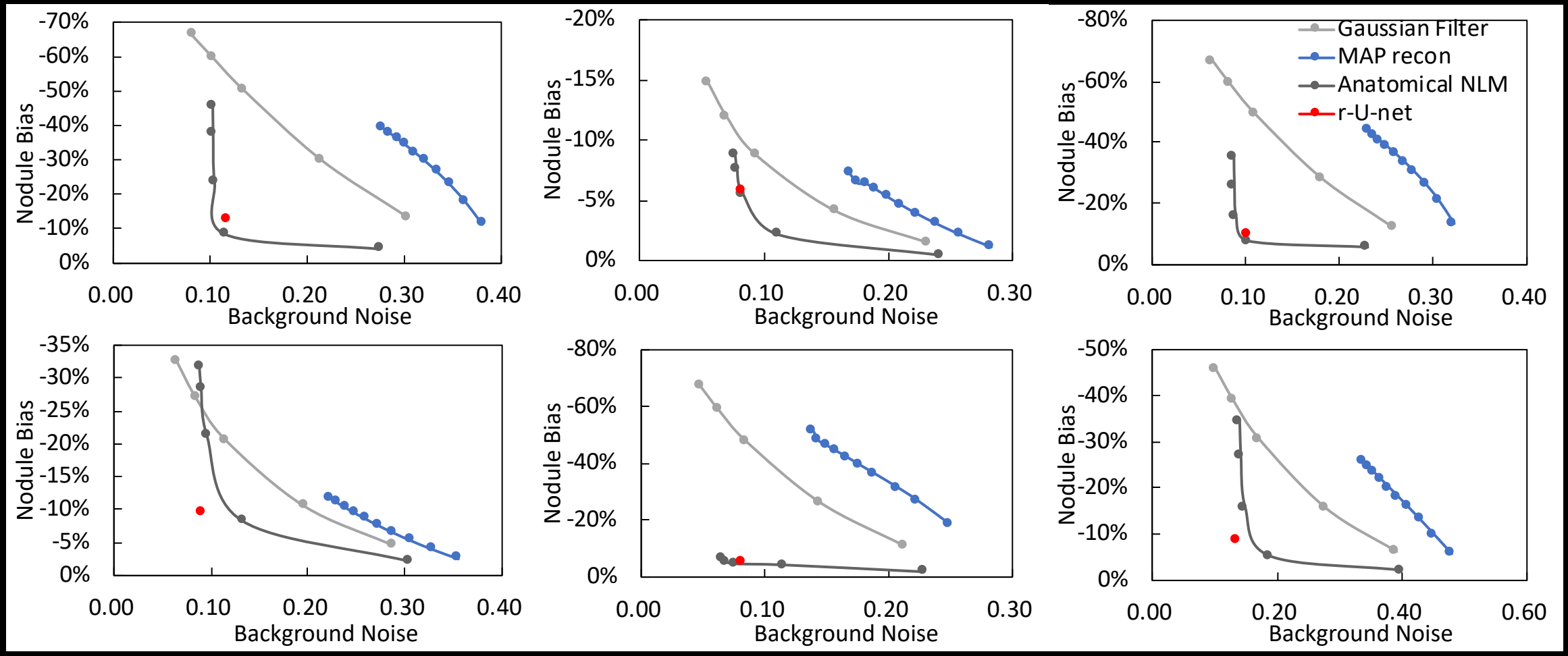

W. Lu, et al. PMB 2019

Comparison between Low Dose PET and Low Dose PET/CT

- 10 patients with CT image and visible nodule in CT image

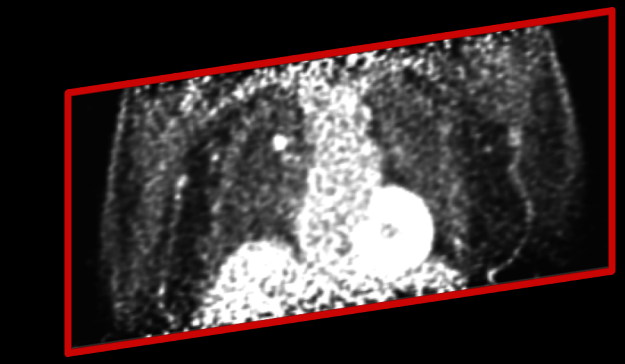

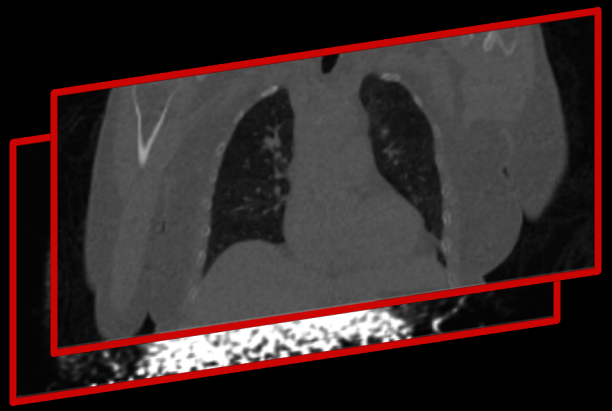

Patch: 64×64×16
Input channel: 1

Patch: 64×64×16×2
Input channel: 2

3D U-Net

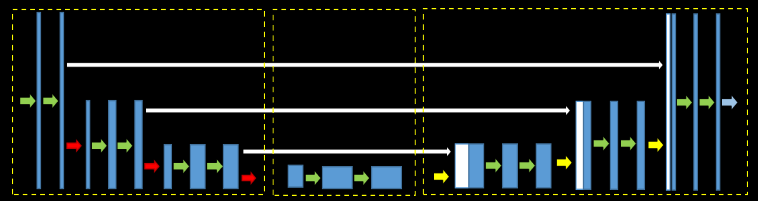

Patch: 64×64×16
Output channel:1

Patch: 64×64×16
Output channel:1

W. Lu, et al. PMB 2019

Comparison between Low Dose PET and Low Dose PET/CT

Patient 4
Slice 190

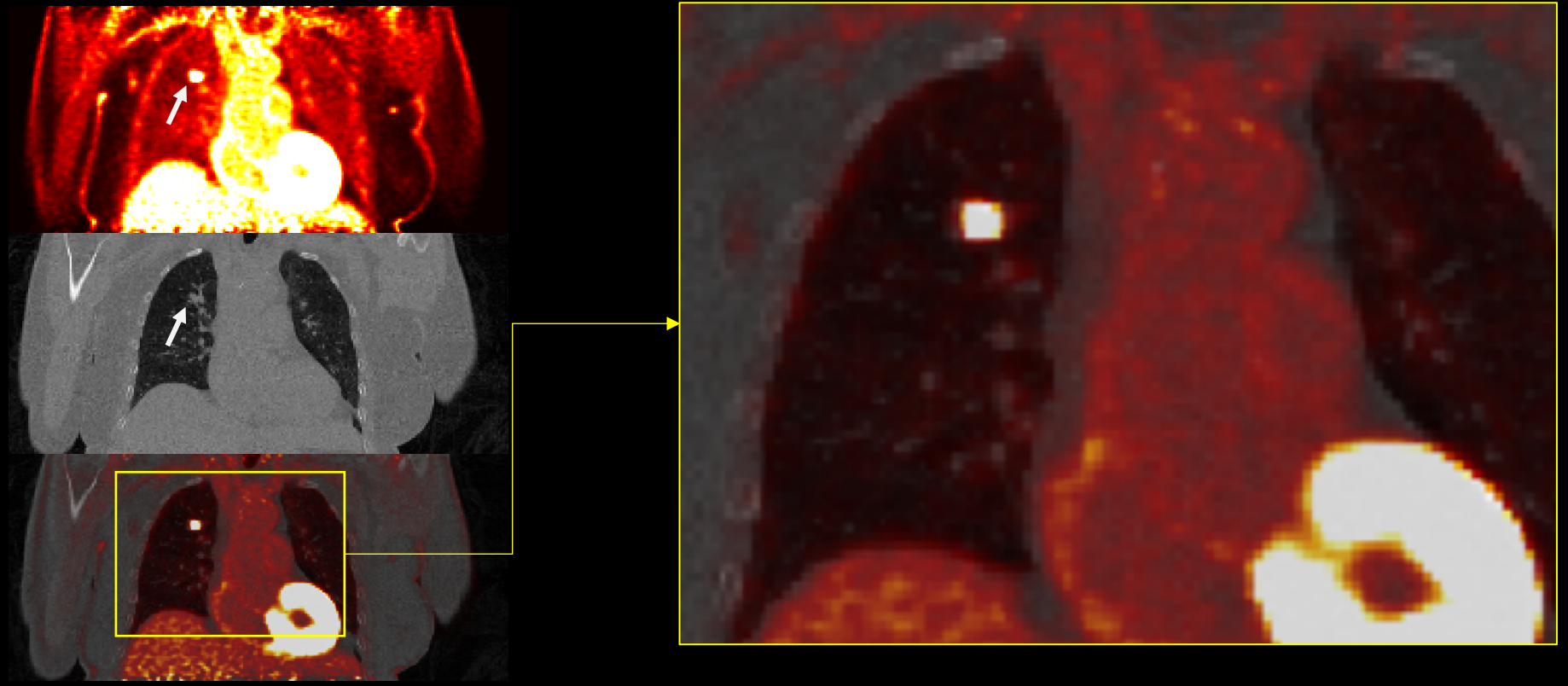

W. Lu, et al. PMB 2019

Comparison between Low Dose PET and Low Dose PET/CT

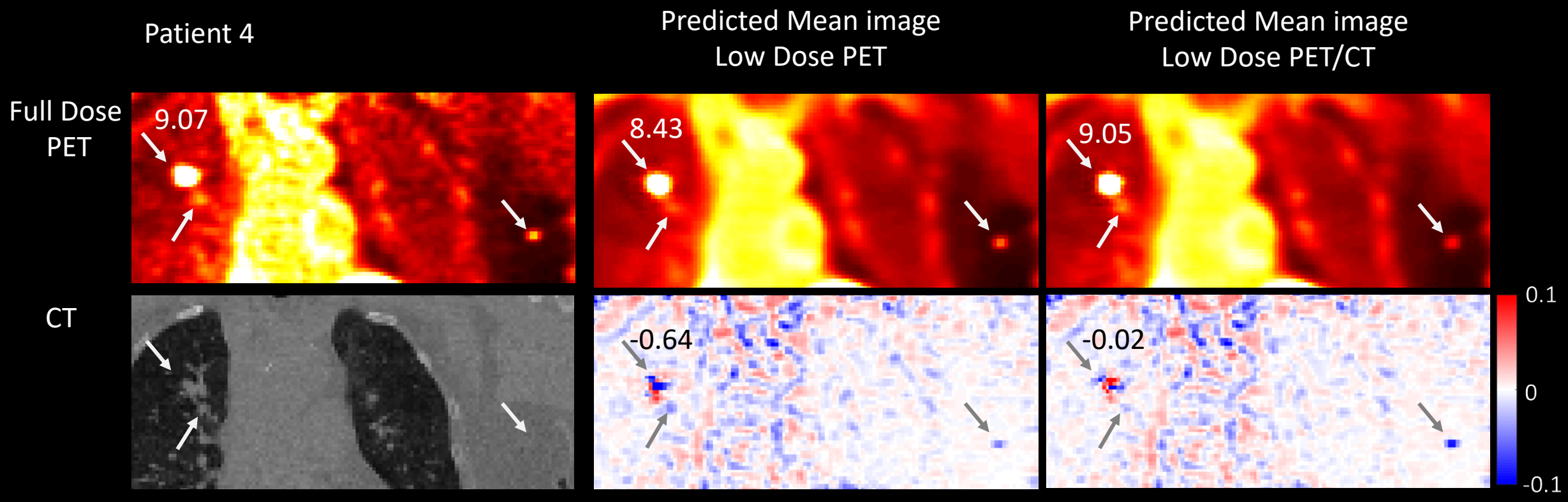

- Nodule bias reduces with well-registered CT information

W. Lu, et al. PMB 2019

Comparison between Low Dose PET and Low Dose PET/CT

Patient 1
Slice 213

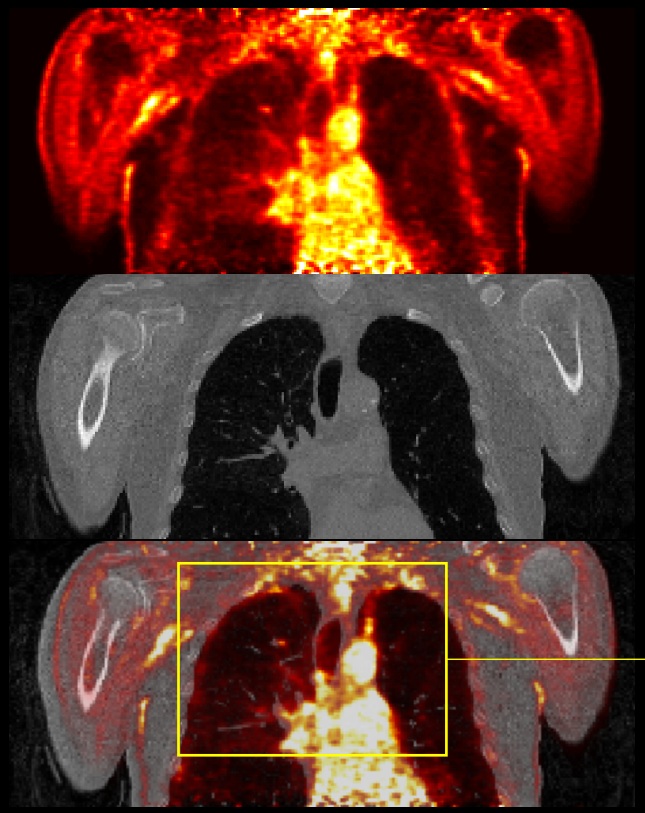

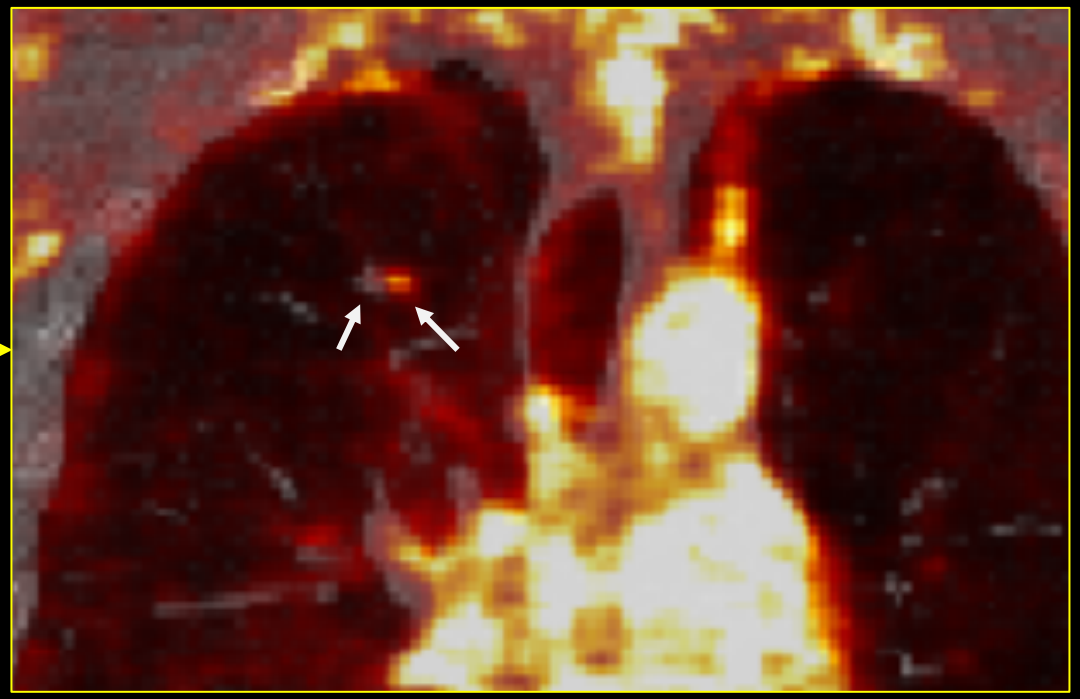

W. Lu, et al. PMB 2019

Comparison between Low Dose PET and Low Dose PET/CT

Patient 1
Slice 217

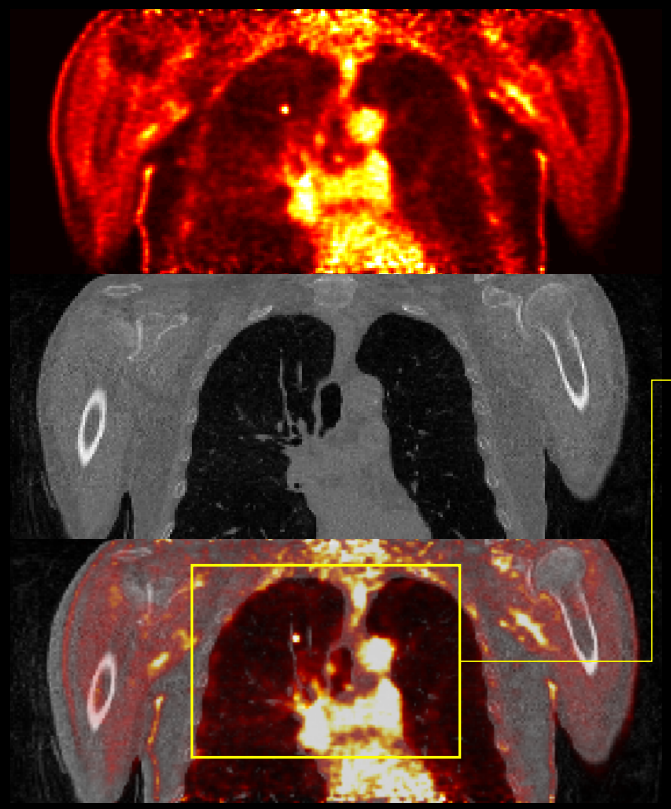

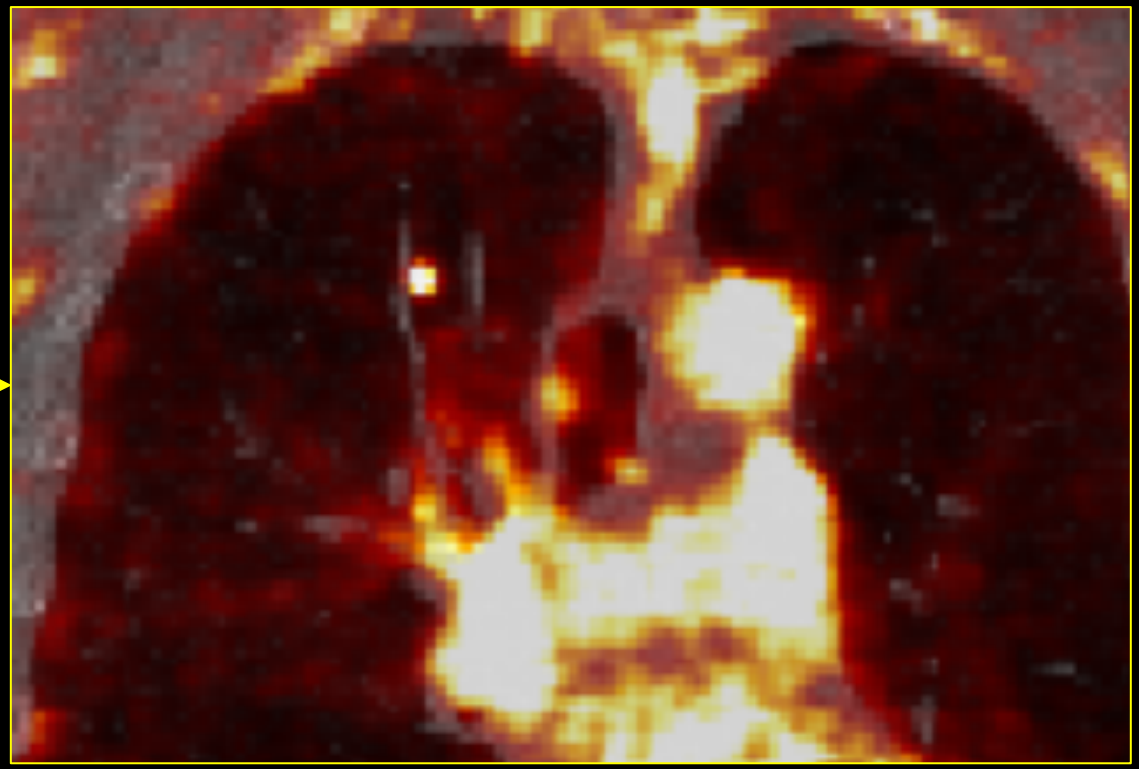

W. Lu, et al. PMB 2019

Comparison between Low Dose PET and Low Dose PET/CT

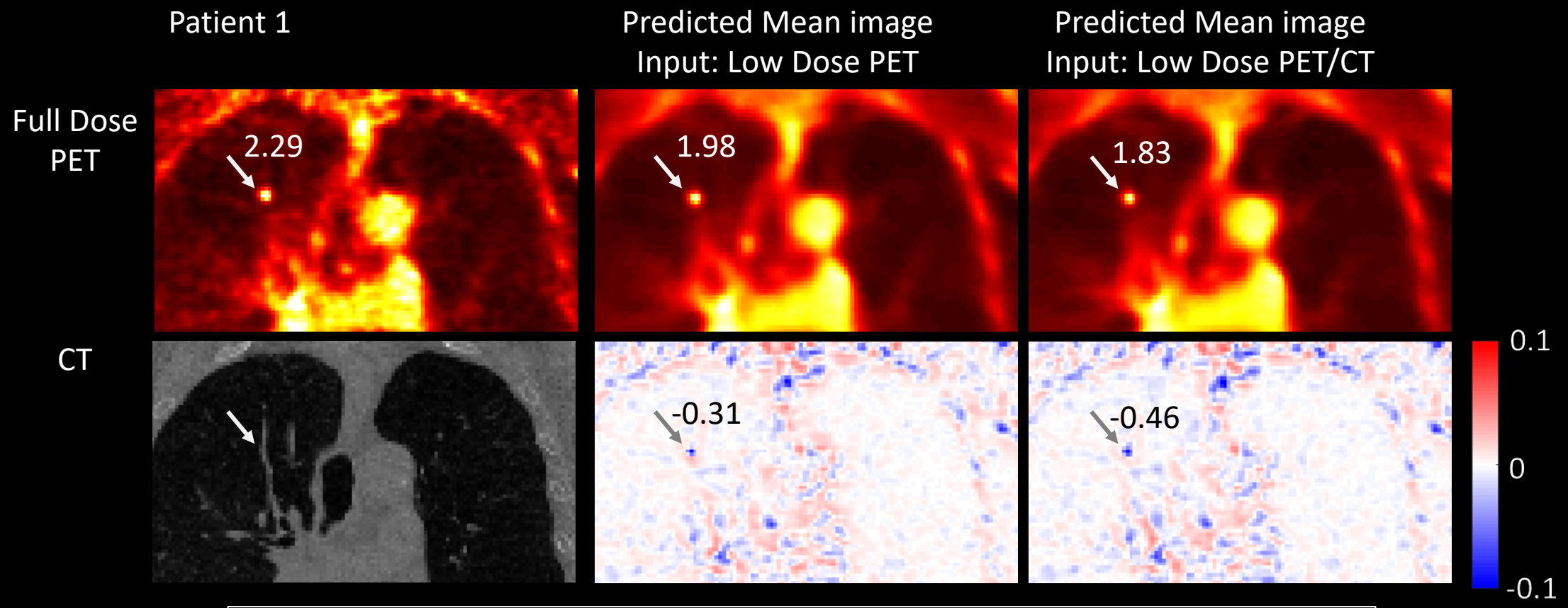

- Mismatch of PET and CT degrades lesion quantification.

W. Lu, et al. PMB 2019

PennPET Explorer: Human studies

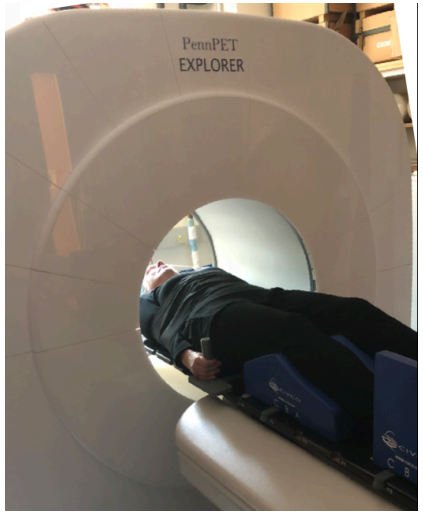

Studies performed with IRB protocol with informed consent

- CT from commercial PET/CT
  - Light restraint of arms and head to aid alignment
  - Register (rigid-body) to non-AC image

- 3 Rings: 70 cm axial length
- Spatial resolution: 4 mm
- TOF resolution: 250 ps
- Sensitivity: 55 kcps/MBq (permits low dose, fast, and late imaging)

PennPET Explorer human studies

- Two subjects were injected with 15 mCi FDG and scanned in a single bed position on PennPET Explorer scanner.

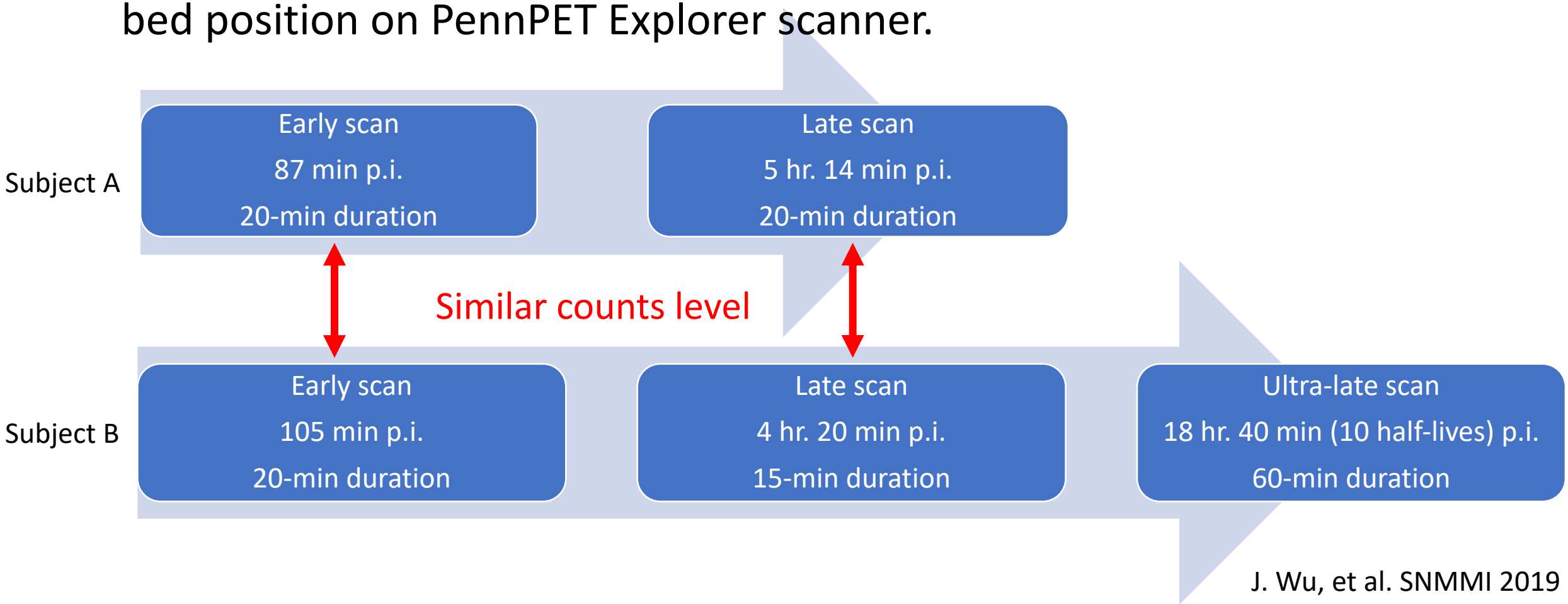

J. Wu, et al. SNMMI 2019

Generate virtual-high-count late and ultra-late images

- No high-count label images of late and ultra-late scans
  - Can we use the high-count early images to train the network?
    - Is the denoising performance affected by FDG distribution?

Image were normalized according to liver uptake

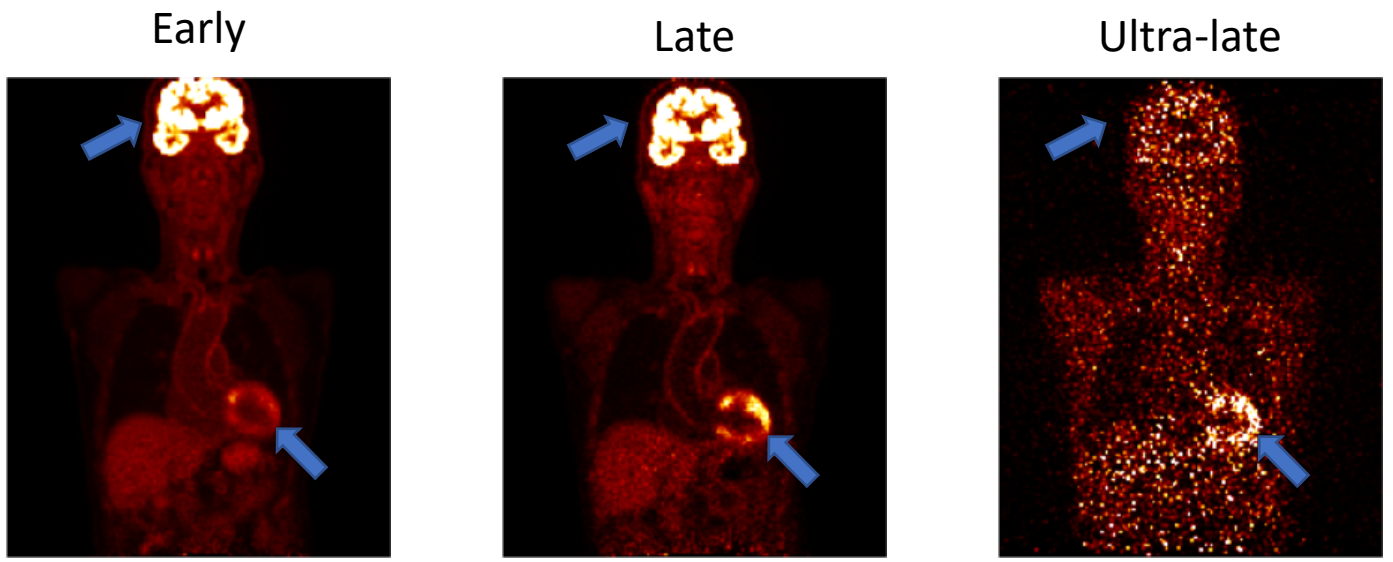

J. Wu, et al. SNMMI 2019

Is denoising performance affected by FDG distribution?

Training network #1 using **late scan** of subject A

- **25% count**
- 4 samples

Input

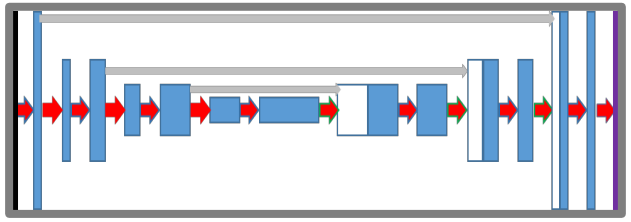

Label

- **100% count**
- 1 sample

Similar counts level

Similar counts level

Training network #2 using **early scan** of subject A

- **6.25% count**
- 4 samples

Input

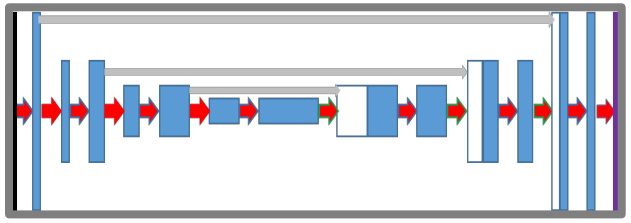

Label

- **25% count**
- 1 sample

Testing network #1 and #2 using **late scan** of subject B

- **25% count**
- 4 samples

Input

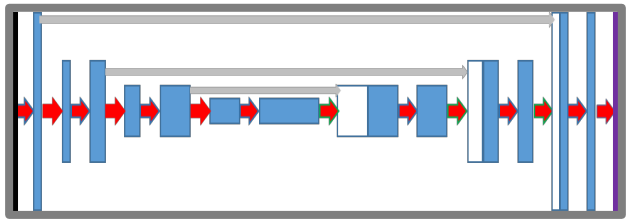

Output

- **Denoised 25% count**
- 4 samples

J. Wu, et al. SNMMI 2019

Image results: is denoising performance affected by FDG distribution?

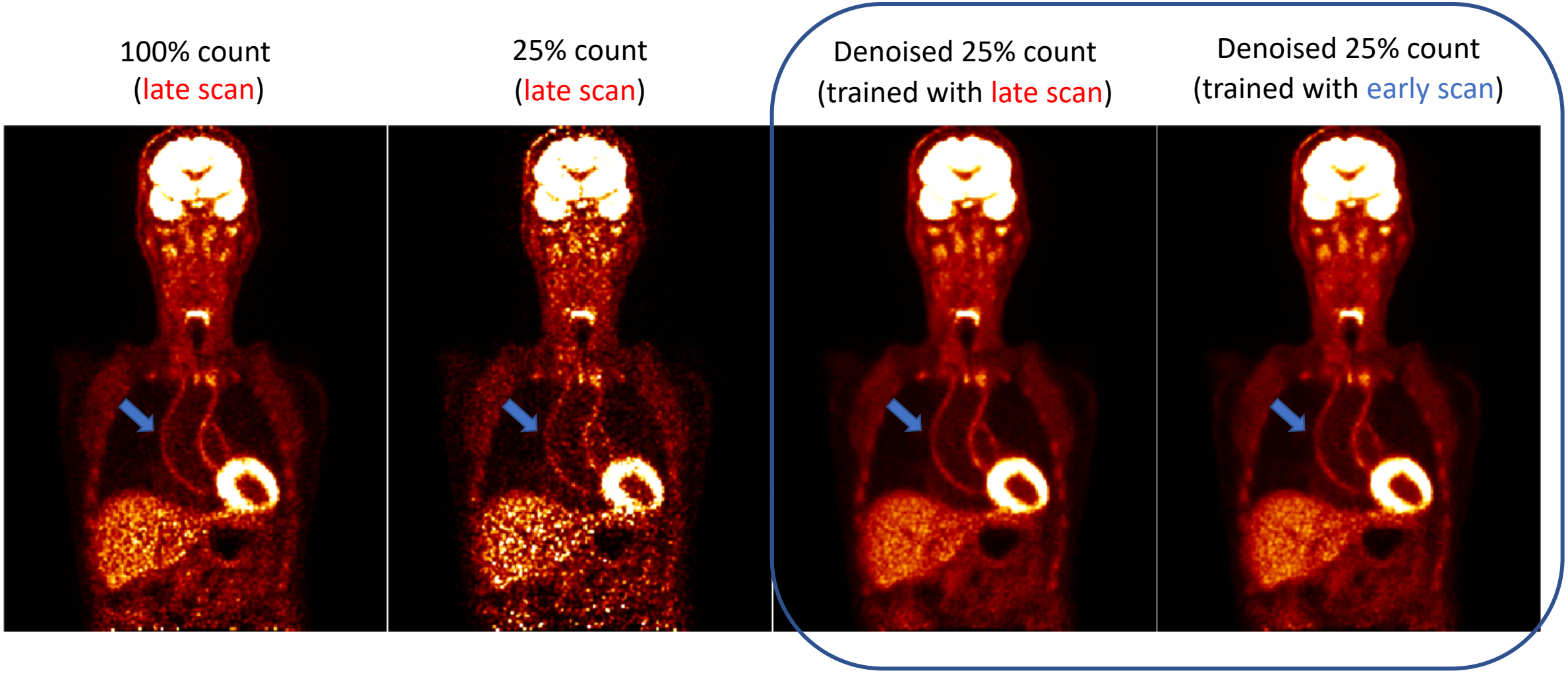

J. Wu, et al. SNMMI 2019

Quantification results:
is denoising performance affected by FDG distribution?

Late scan	Noise (std/mean)	Relative bias compared to 100% count					CNR
	Liver	Cerebellum	Bone marrow	Myocardium	Aorta wall	Inflammation	Inflammation
100% count	0.20	-	-	-	-	-	6.9
25% count	0.37±0.01	0%±1%	-1%±3%	0%±0%	-1%±0%	-1%±2%	3.7±0.1
Denoised 25% (trained with late scan)	0.10±0.002	-2%±1%	-3%±2%	-1%±0%	-3%±0%	-2%±2%	13.1±0.2
Denoised 25% (trained with early scan)	0.10±0.002	-2%±0%	-4%±2%	-1%±0%	-4%±0%	-4%±2%	12.5±0.4

Generate virtual-high-count late image

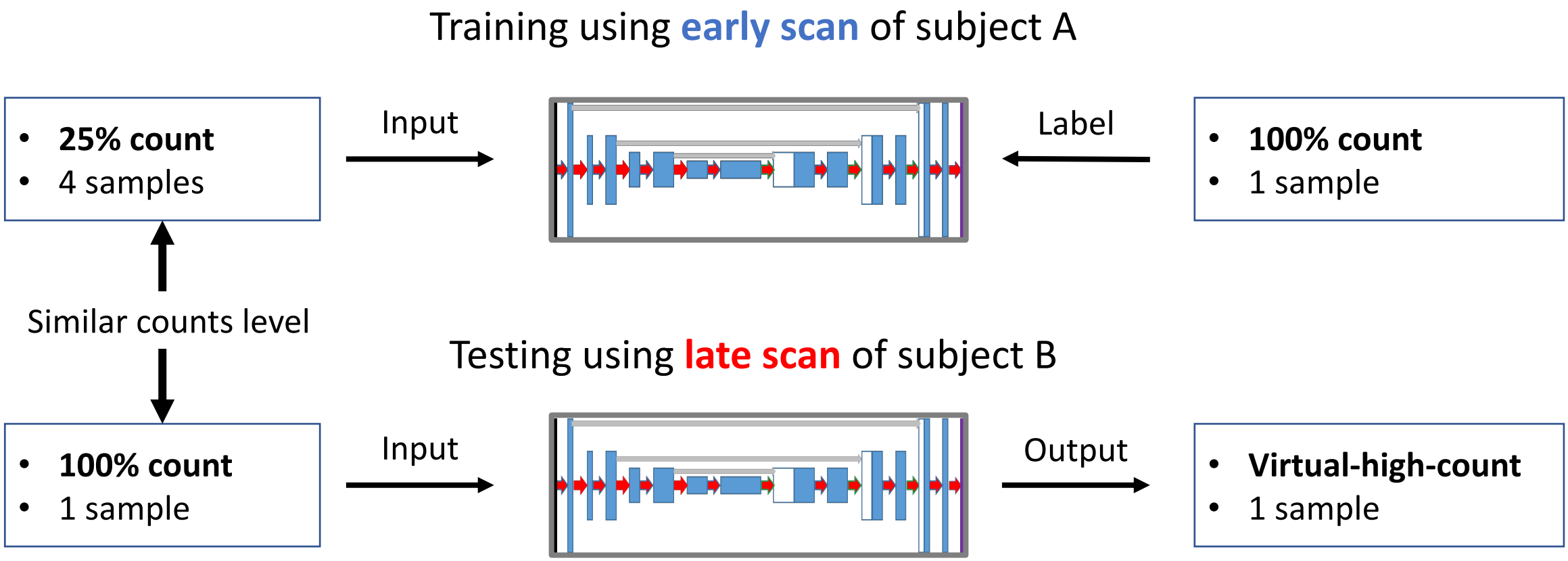

J. Wu, et al. SNMMI 2019

Results: generate virtual-high-count late image

100% count (late scan)

Virtual-high-count (late scan)

100% count (late scan)

Virtual-high-count (late scan)

Late scan	Noise (std/mean)	Relative bias compared to 100% count					CNR
	Liver	Cerebellum	Bone marrow	Myocardium	Aorta wall	Inflammation	Inflammation
100% count	0.20	-	-	-	-	-	6.9
Virtual-high-count	0.07	0%	-1%	-1%	-3%	-2%	18.1

Generate virtual-high-count ultra-late image

Training using **early scan** of subject A

- **0.24% count**
- 20 samples

Input

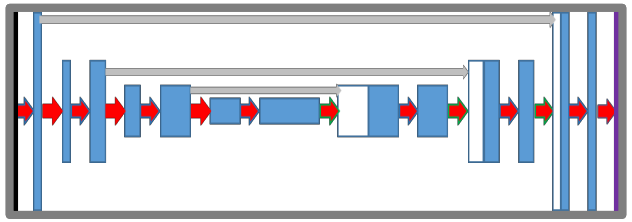

Label

- **100% count**
- 1 sample

Similar counts level

Testing using **ultra-late scan** of subject B

- **100% count**
- 1 sample

Input

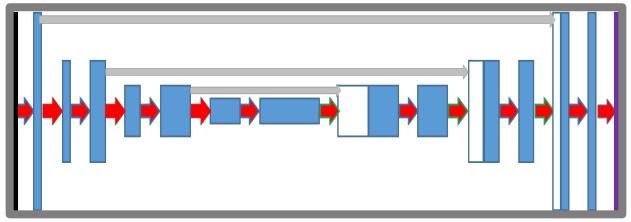

Output

- **Virtual-high-count**
- 1 sample

J. Wu, et al. SNMMI 2019

Results: generate virtual-high-count ultra-late image

100% count (ultra-late scan) | Virtual-high-count (ultra-late scan)

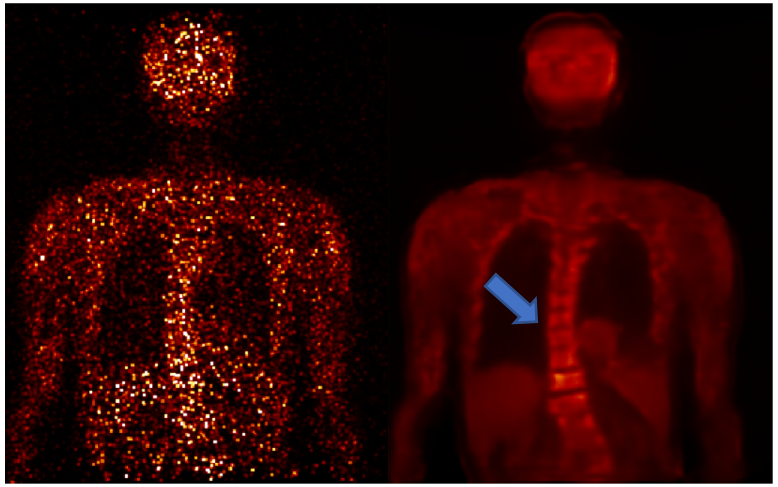

100% count (ultra-late scan) | Virtual-high-count (ultra-late scan)

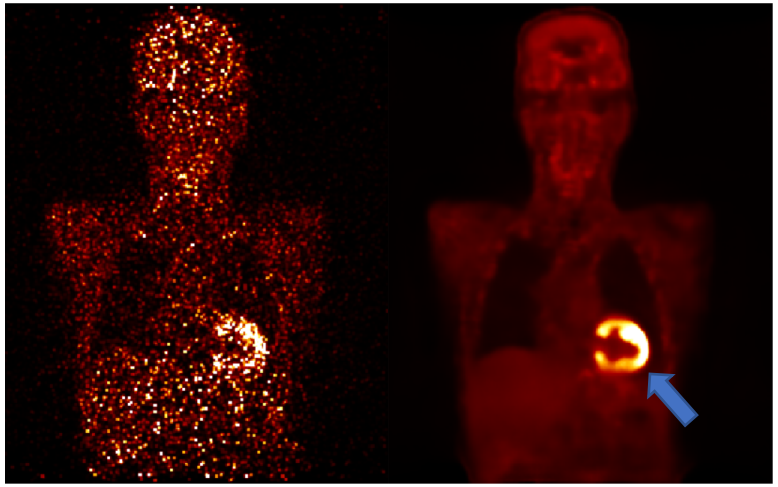

100% count (ultra-late scan) | Virtual-high-count (ultra-late scan)

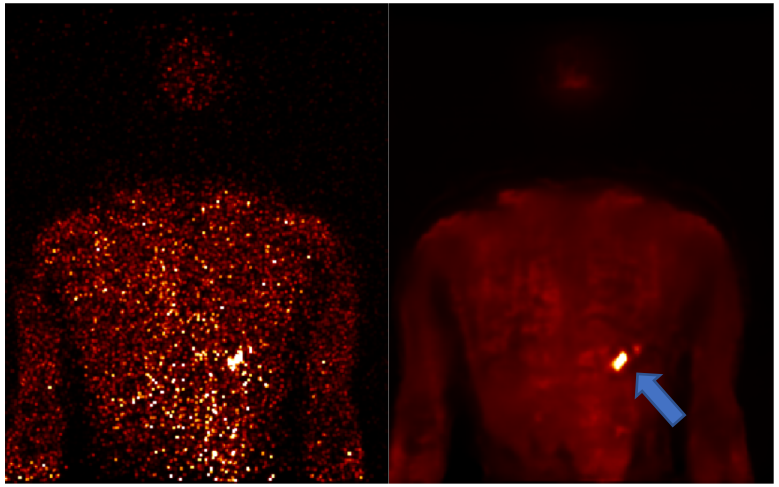

Ultra-late scan	Noise (std/mean)	Relative bias compared to 100% count			CNR
	Liver	Bone marrow	Myocardium	Inflammation	Inflammation
100% count	1.08	-	-	-	3.1
Virtual-high-count	0.04	-5%	1%	-25%	53.4

Limitation for Non-FDG tracers

- Tracer with short half-lives
  - O-15: 122.2 s
  - Rb-82: 76.4 s
- Tracer with long half-lives
  - Zr-89: 3.27 days

- Full dose images may not be available!

- New tracers
- Uncommonly used tracers

- Training dataset may not be sufficient!

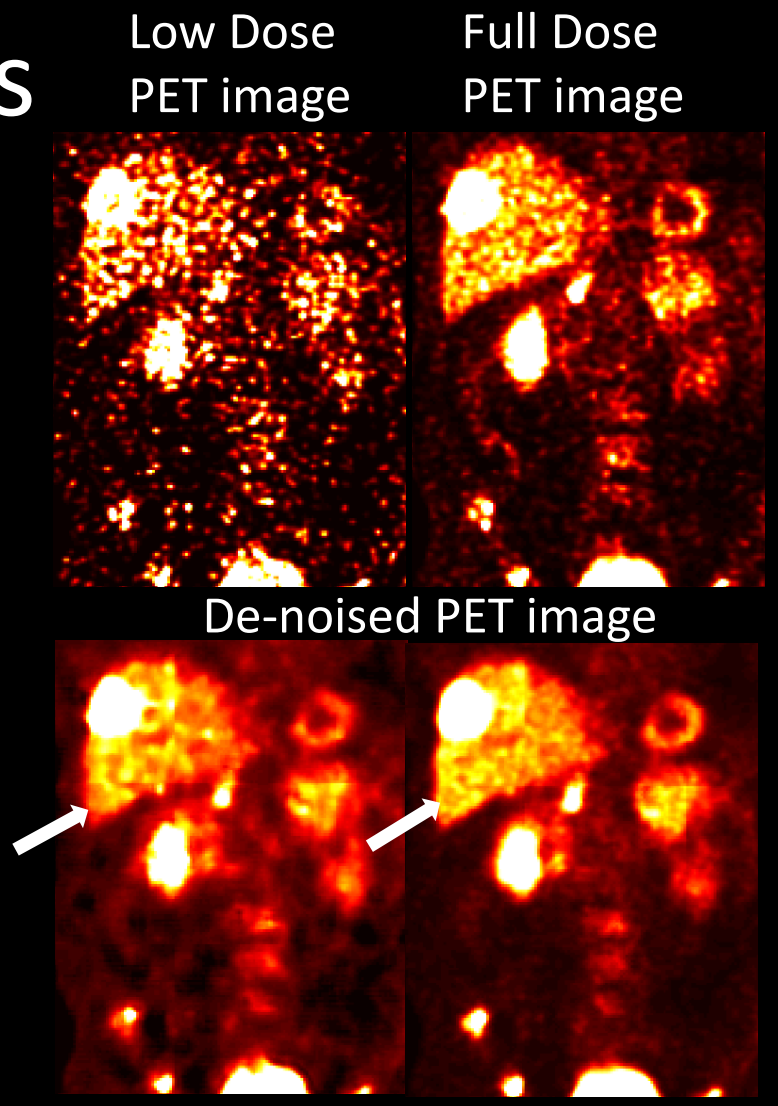

H. Liu, et al. SNMMI 2019

Training and testing: Single bed

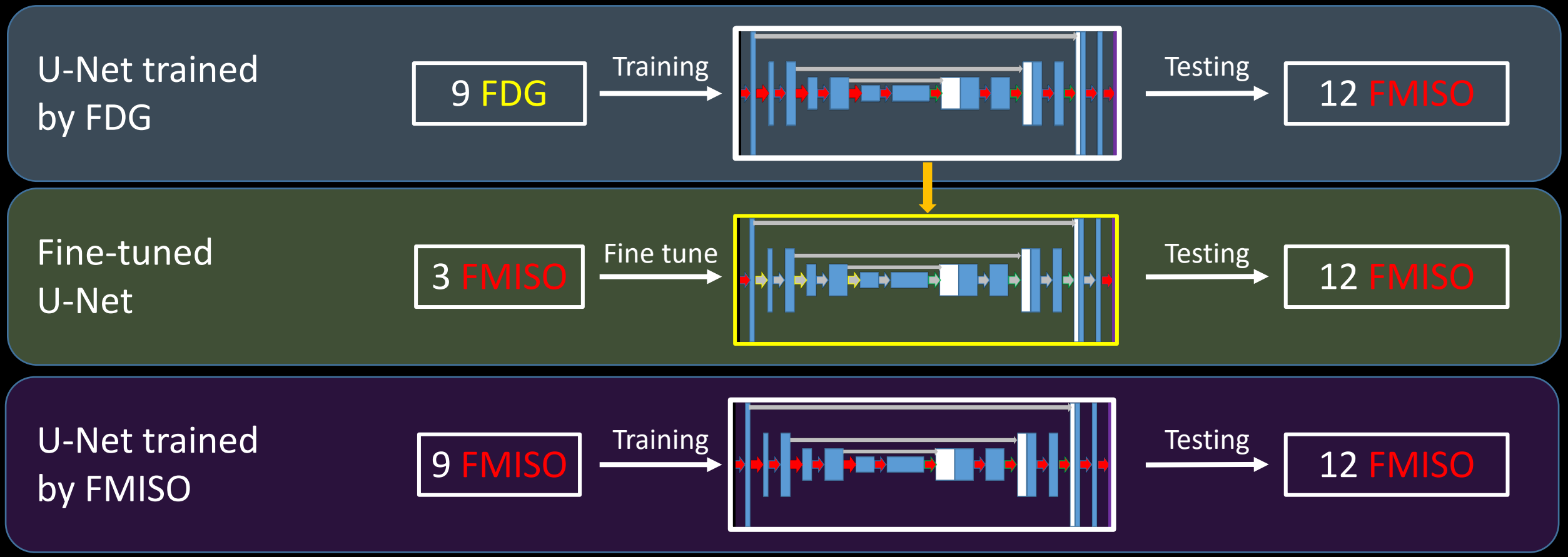

Fine tune: only the first layer and final layer would be updated.

For Fine-tuned U-Net and U-Net trained by FMISO:
Leave out cross-validation approach was used.

Sample slices: Single bed FMISO

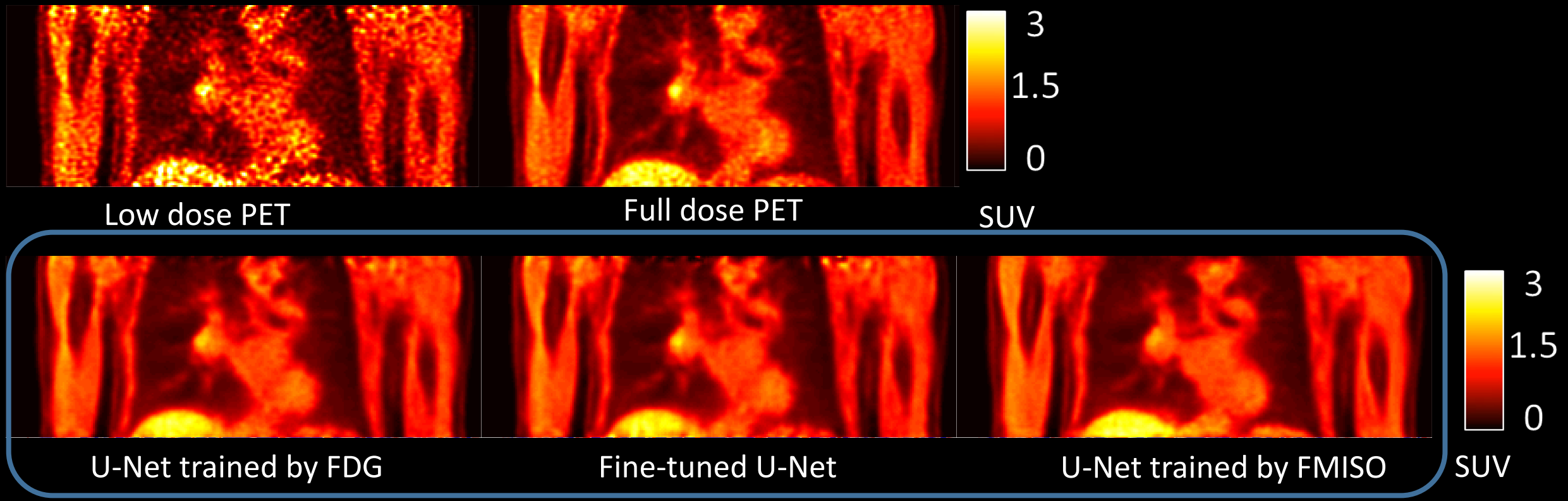

The de-noised image with the three U-Nets are comparable!

Whole body FDG and DOTATATE

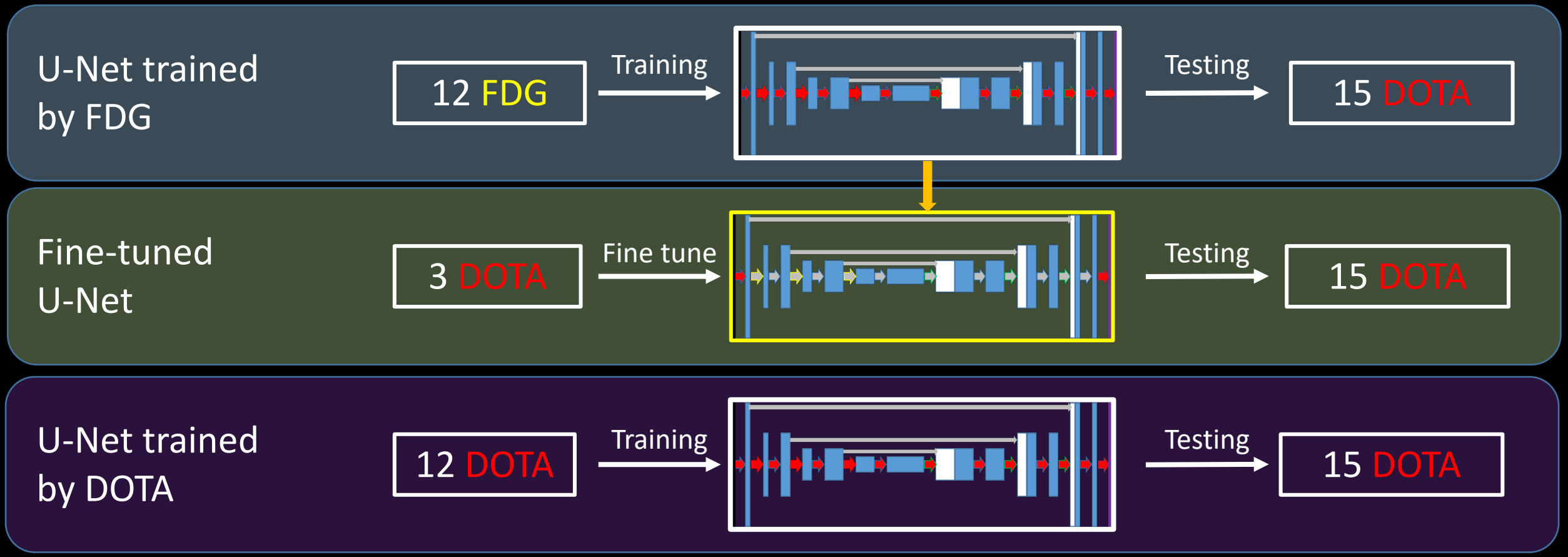

Fine tune: only the first layer and final layer would be updated.

For Fine-tuned U-Net and U-Net trained by DOTA: Leave out cross-validation approach was used. .

Sample slices: Whole body DOTATATE

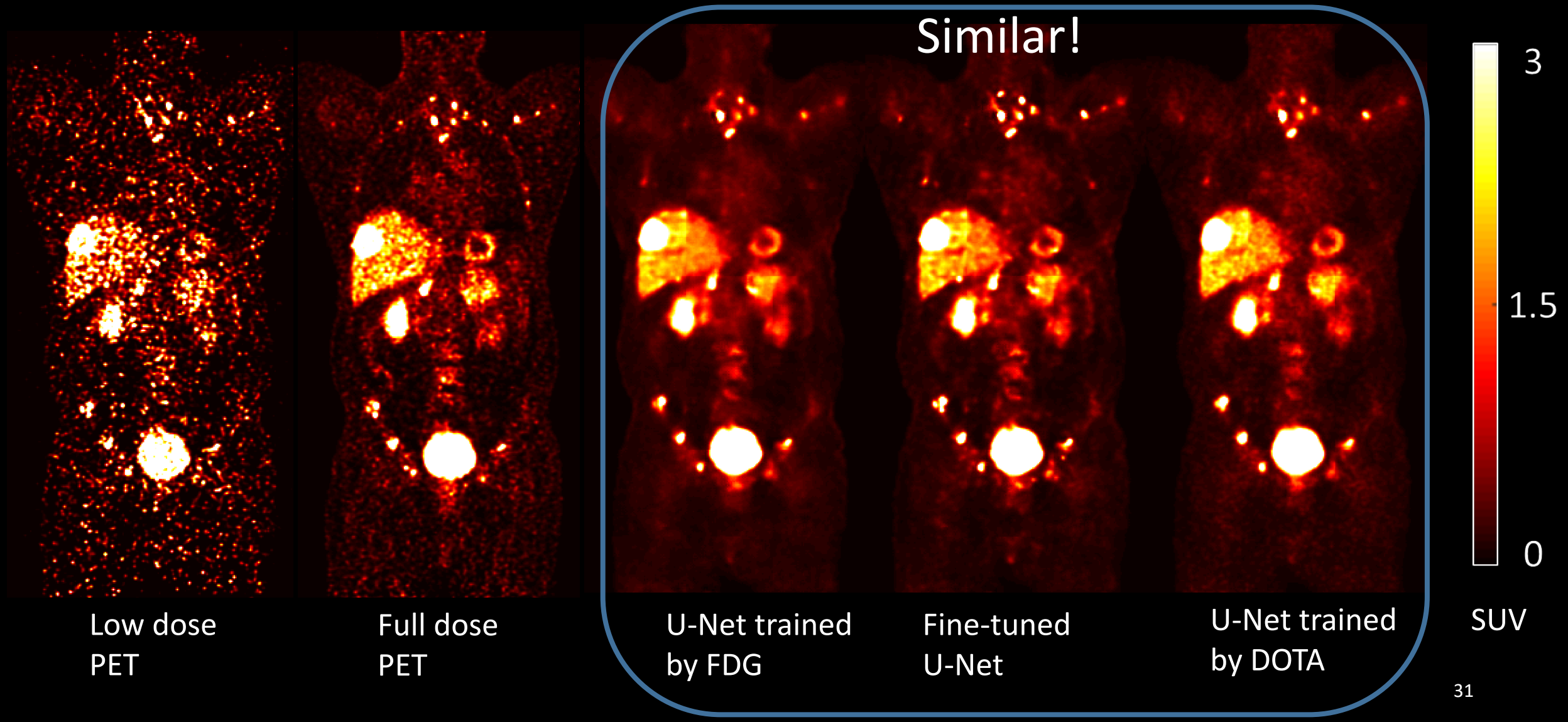

Cross-tracer & cross-protocol transfer learning

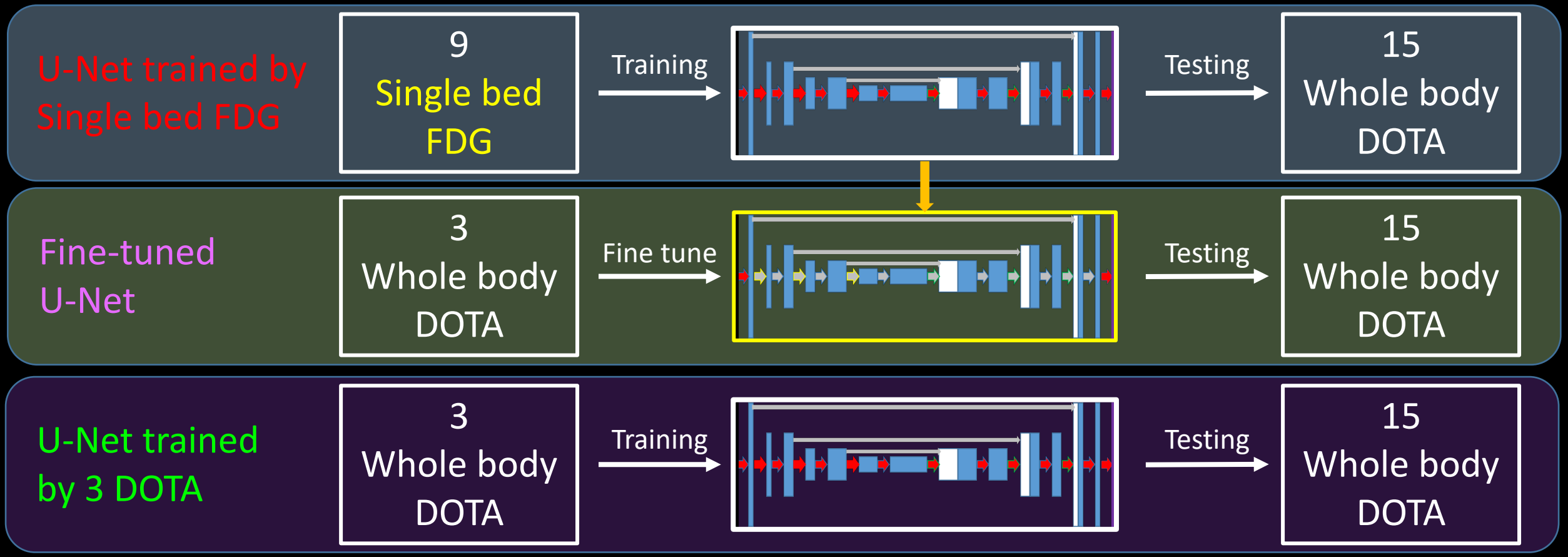

U-Net trained by 12 DOTA was used as reference.

Fine tune: only the first layer and final layer would be updated.

For Fine-tuned U-Net and U-Net trained by 3 DOTA:
Leave out cross-validation approach was used.

Cross-tracer & cross-protocol transfer learning

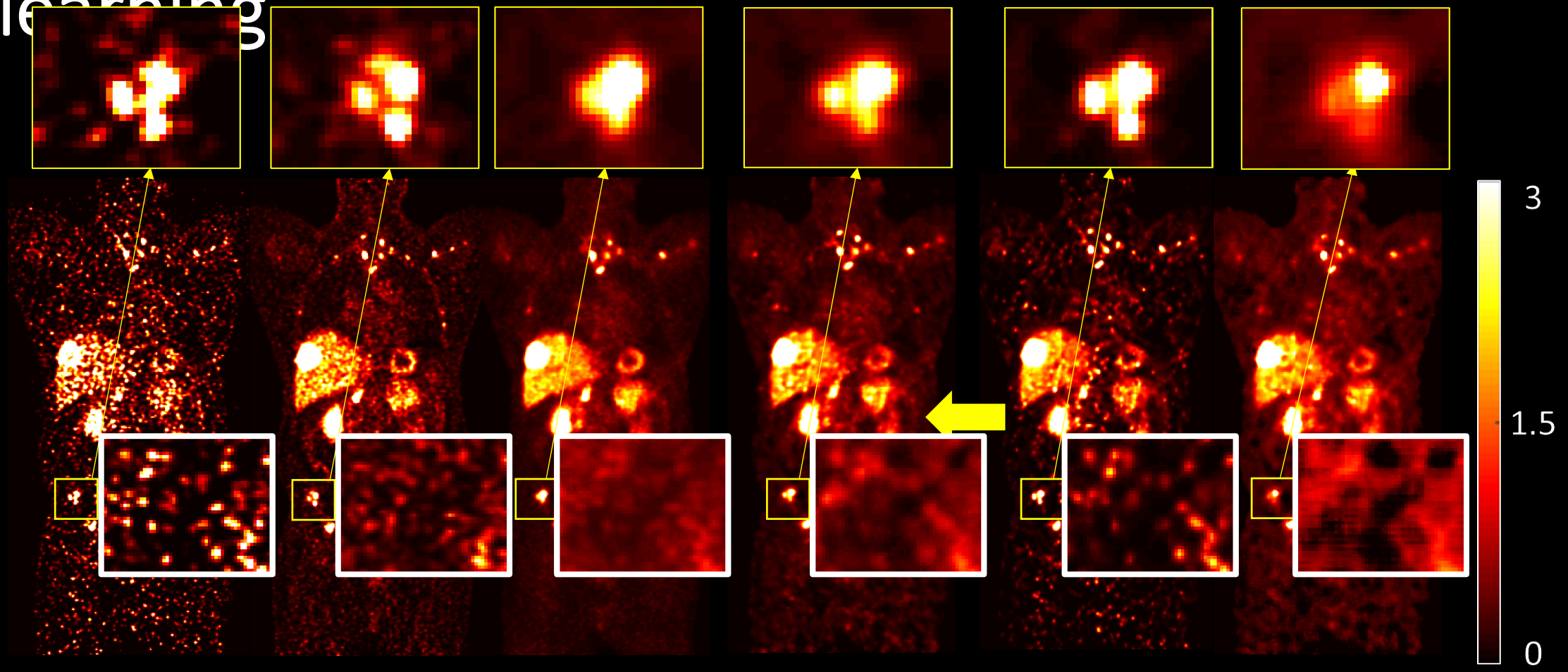

Low dose PET

Full dose PET

U-Net trained by 12 whole body DOTA

Fine-tuned U-Net with 3 whole body DOTA

U-Net trained by 9 single bed FDG

U-Net trained by 3 whole body DOTA

Brain PET Imaging

- Positron Emission Tomography (PET) imaging is increasingly employed in AD studies to measure β-amyloid, tau protein, glucose metabolism, synaptic vesicle glycoprotein 2A (SV2A) and so on.

Isotope	Tracer	Tracer Description
^{18}F	**FDG**	**glucose metabolism**
^{18}F	**AV-1451**	**tau imaging agent**
^{11}C	**PiB**	**β-amyloid**
^{11}C	**UCB-J**	**Synaptic Vesicle 2A (SV2A) ligand**

Static Images of four tracers from One AD Patient

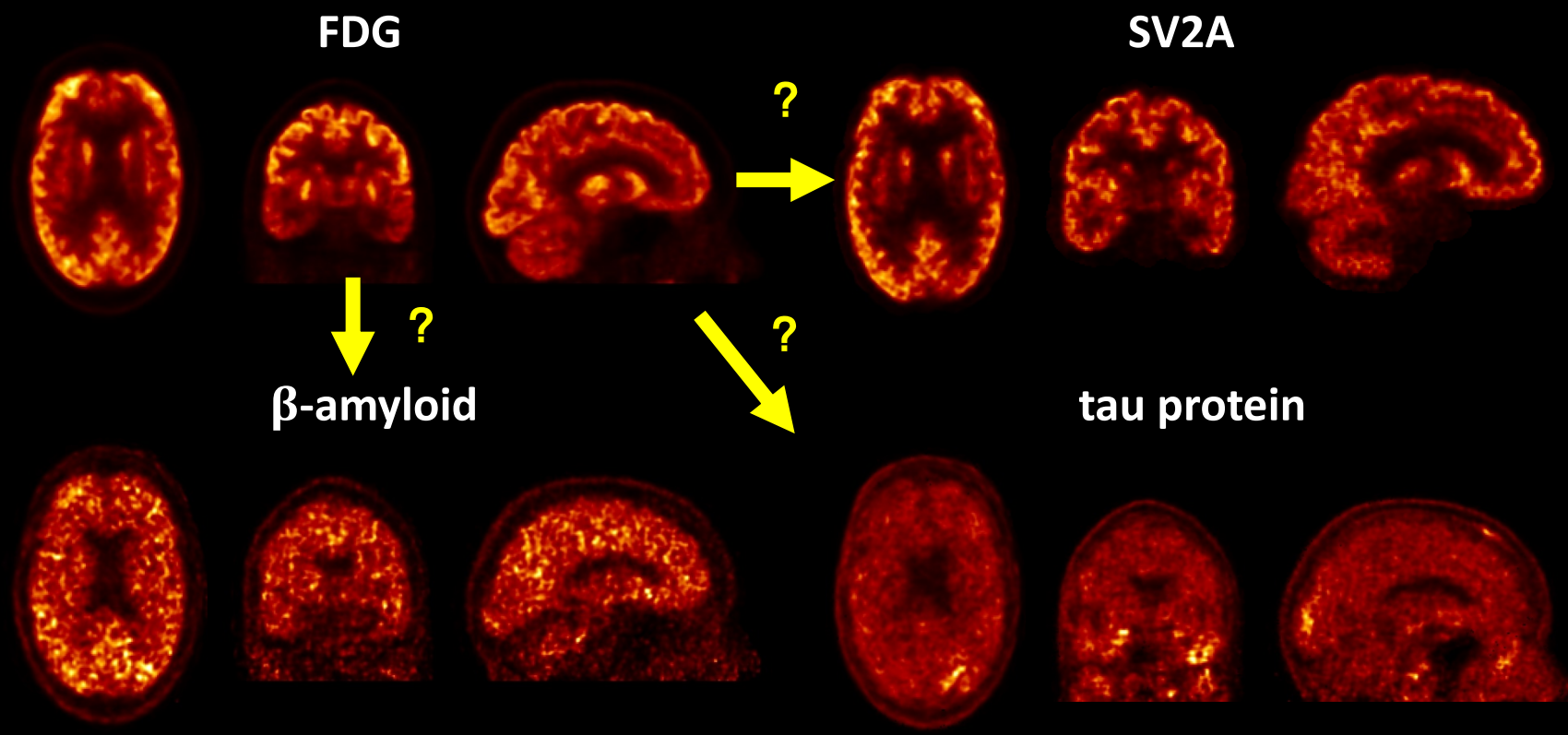

Index of Network		SV2A output	
		SUVR	BP_{nd} ratio
FDG input	SUVR	#1	#3
	K_i Ratio	#2	#4

Static Image Prediction

Network #1: SUVR->SUVR

Network #2: K_i ratio->SUVR

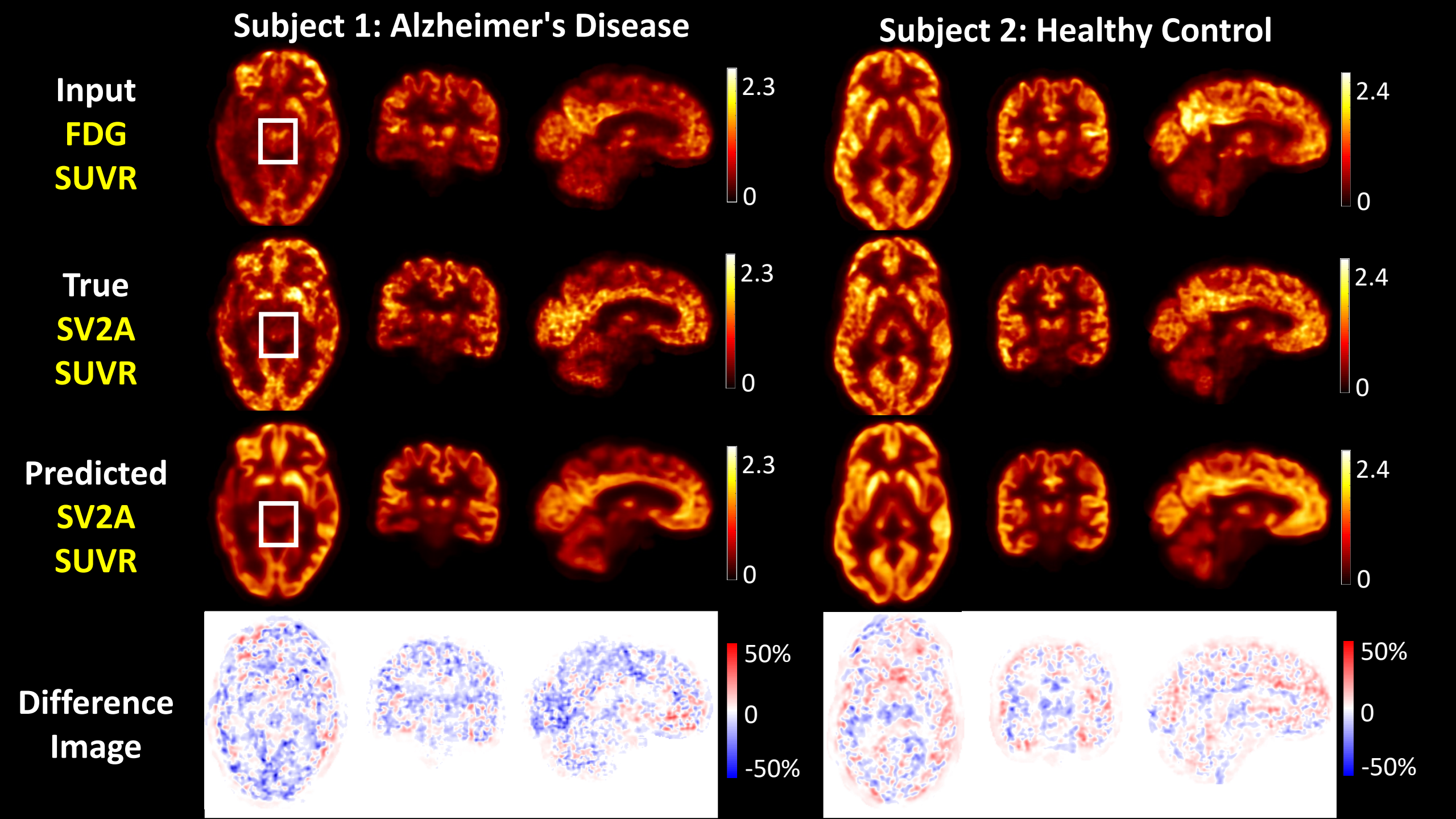
Subject 1: Alzheimer's Disease
Subject 2: Healthy Control
Input
FDG
SUVR
True
SV2A
SUVR
Predicted
SV2A
SUVR
Difference
Image
2.3
0
2.4
0
50%
0
-50%

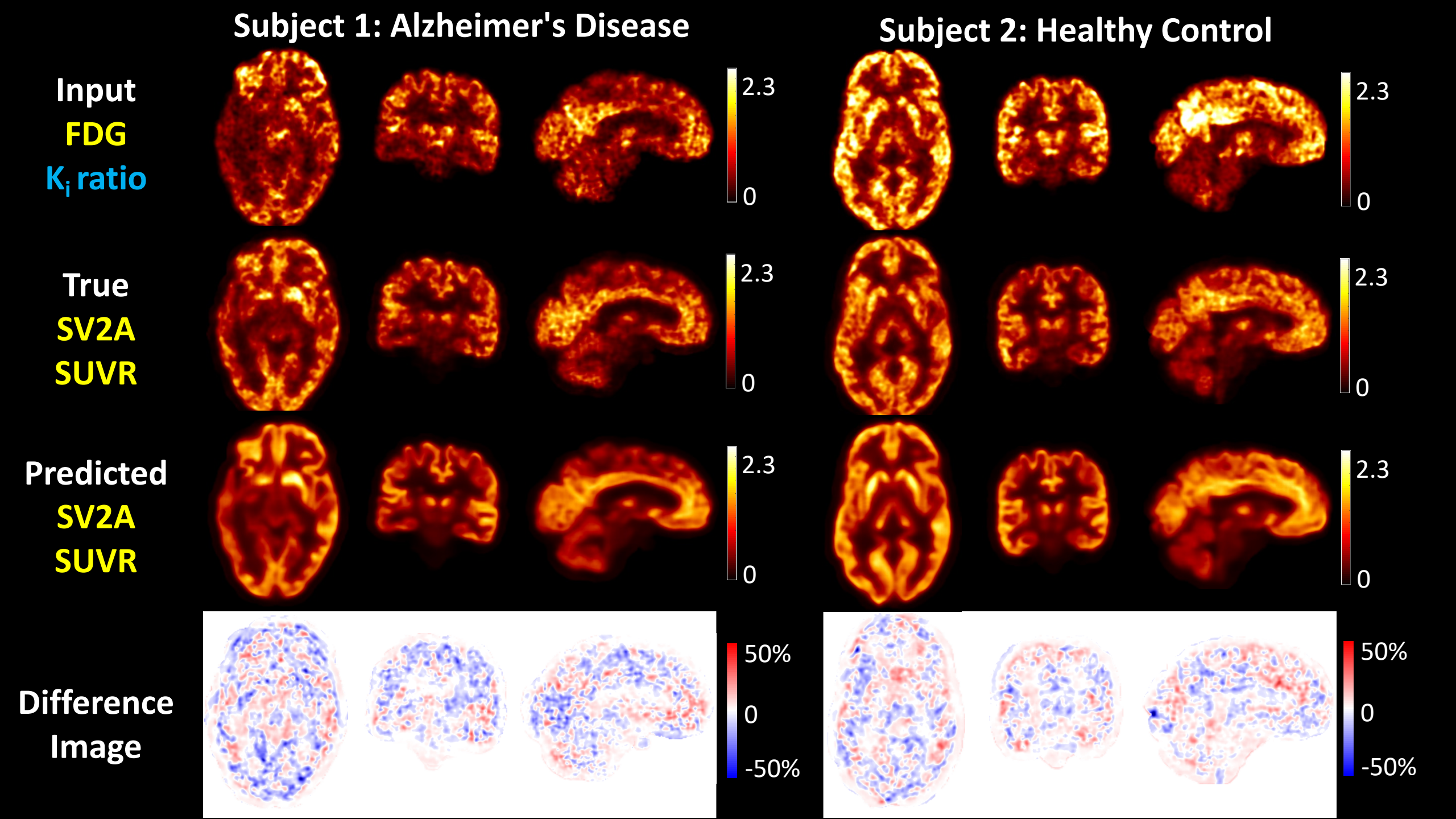
Subject 1: Alzheimer's Disease
Subject 2: Healthy Control
Input
FDG
K_i ratio
True
SV2A
SUVR
Predicted
SV2A
SUVR
Difference
Image
2.3
0
50%
0
-50%

SUVR -> SUVR VS K_i ratio -> SUVR

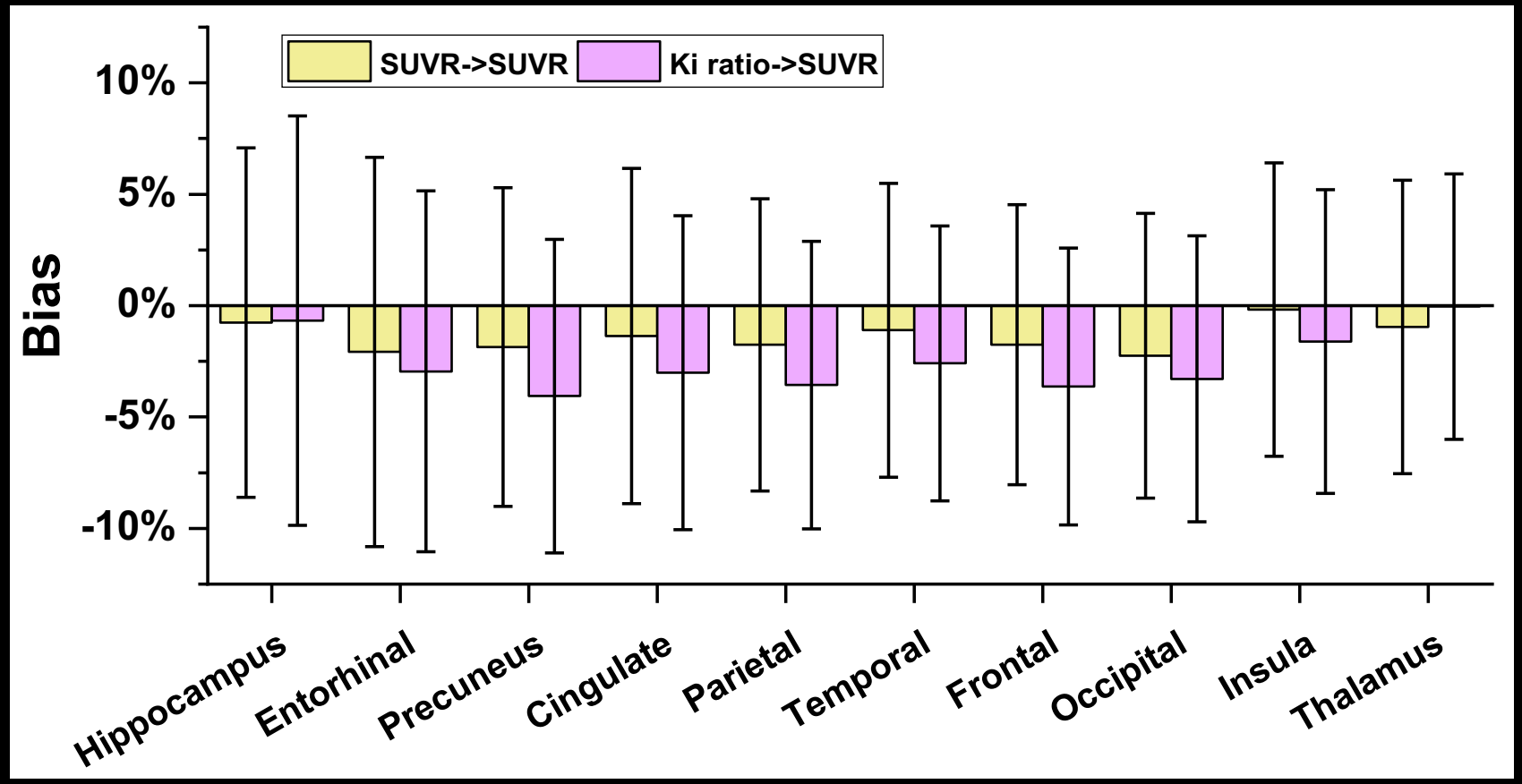

Mean bias across all the 18 ROI

Network	Mean±SD
SUVR->SUVR	-0.4%±6.8%
K_i ratio->SUVR	-0.9%±7.0%

- Both SUVR and K_i ratio of FDG can provide robust prediction of SV2A SUVR.
- SUVR is slightly better, and is preferred as input for its easy of use

FDG —> β-amyloid

#Network1 SUVR->SUVR

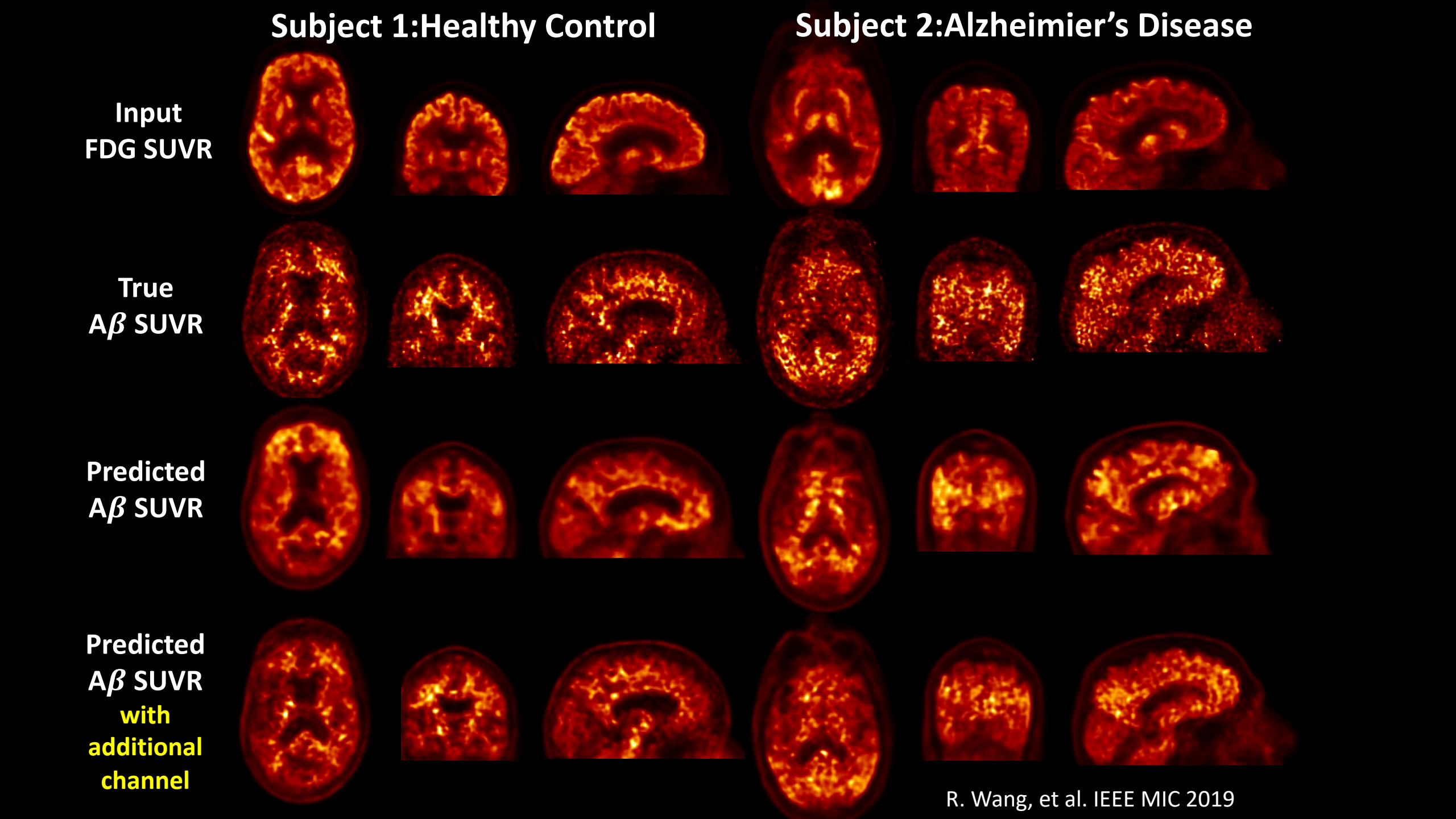
Subject 1:Healthy Control
Subject 2:Alzheimier's Disease
Input FDG SUVR
True Aβ SUVR
Predicted Aβ SUVR
Predicted Aβ SUVR with additional channel
R. Wang, et al. IEEE MIC 2019

Summary

- SPECT
  - Attenuation Map Generation
  - Direct Attenuation Correction
- PET
  - Denoising
  - Motion Correction
    - simultaneous denoising and motion estimation
  - Multi-tracer Image Generation
    - FDG -> other AD tracer

Acknowledgement

Group Member
Luyao Shi
Jing Wu
Hui Liu
Rui Wang
Bo Zhou
Wenzhuo Lu
Yu-Jung Tsai

PET Center
Richard Carson
Zhongdong Sun
Tak Toyonaga
Nozomi Sumida
Maribel Rayas
Tara Zalatimo

YNHH
Ming-Kai Chen
Larry Saperstein
David Menard
Joseph Ankrah
Matthew Gregory

Imaging Processing and Analysis
John Onofrey
Xenios Papademetris
Nicha Dvornek
Jim Duncan

University of Pennsylvania
Joel Karp
Margaret Daube-Witherspoon

Funding
R01EB025468
R01CA224140
R01HL123949